Accepted Manuscript

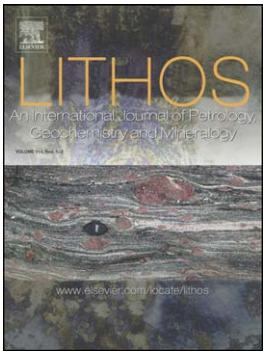

Geochemistry, Sr-Nd-Pb isotopes and geochronology of amphibole- and mica-bearing lamprophyres in northwestern Iran: Implications for mantle wedge heterogeneity in a paleo-subduction zone

Mehraj Aghazadeh, Dejan Prelević, Zahra Badrzadeh, Eleonora Braschi, Paul van den Bogaard, Sandro Conticelli

PII: S0024-4937(15)00007-9
DOI: doi: 10.1016/j.lithos.2015.01.001
Reference: LITHOS 3485

To appear in: *LITHOS*

Received date: 4 April 2014
Accepted date: 3 January 2015

Please cite this article as: Aghazadeh, Mehraj, Prelević, Dejan, Badrzadeh, Zahra, Braschi, Eleonora, van den Bogaard, Paul, Conticelli, Sandro, Geochemistry, Sr-Nd-Pb isotopes and geochronology of amphibole- and mica-bearing lamprophyres in northwestern Iran: Implications for mantle wedge heterogeneity in a paleo-subduction zone, *LITHOS* (2015), doi: 10.1016/j.lithos.2015.01.001

Geochemistry, Sr-Nd-Pb isotopes and geochronology of amphibole- and mica-bearing lamprophyres in northwestern Iran: implications for mantle wedge heterogeneity in a paleo-subduction zone

Mehraj Aghazadeh[1], Dejan Prelević[2], Zahra Badrzadeh[1], Eleonora Braschi[3], Paul van den Bogaard[4], and Sandro Conticelli[3,5]

[1] *Department of Geology, Payame Noor University, Iran*

[2] *Institut für Geowissenschaften, Johannes Gutenberg-Universität Mainz J.-J.-Becher-Weg, 21, D-55099 Mainz, Germany*

[3] *Research Unit of Florence, Istituto di Geoscienze e Georisorse, C.N.R., Via Giorgio La Pira, 4, I-50121, Firenze, Italy*

[4] *GEOMAR Helmholtz-Zentrum für Ozeanforschung Kiel,,Wischhofstraße, 1-3, D-24148, Kiel, Germany*

[5] *Dipartimento di Scienze della Terra, Università degli Studi di Firenze, Via Giorgio La Pira, 4, I-50121, Firenze, Italy*

Abstract

Lamprophyres of different age showing distinctive mineralogy, geochemistry and isotopic ratios are exposed in northwestern Iran. They can be divided into Late Cretaceous sannaite, Late Oligocene-Early Miocene camptonite (amphibole-bearing) and Late Miocene minette (mica-bearing) and spessartite (amphibole-bearing) lamprophyres.

Sannaites have high-Ti amphibole along with high-Ti and Al clinopyroxene, and they are characterised by homogeneous enrichment in incompatible trace elements with troughs at Pb. Spessartites have hornblende and low-Al and Ti clinopyroxene, and they are characterised by enriched incompatible trace element pattern with depletions of Nb, Ta, Pb, and Ti with respect to large ion lithophile elements. Minettes have high-Ti and Al brown mica and low-Al and Ti clinopyroxene, and similarly to spessartite, are characterised by fractionation of high field strength elements with respect to large ion lithophile elements, with troughs at Nb, Ta, and Ti and a peak at Pb. Minettes show high initial $^{87}Sr/^{86}Sr$ values up to 0.70760 and low initial $^{143}Nd/^{144}Nd$ down to 0.512463 with a negative correlation, consistent with the trace element distribution related with an enriched mantle source modified after sediment recycling during subduction and continental collision.

Cretaceous sannaites and Early Miocene spessartites show low initial $^{87}Sr/^{86}Sr$ approaching 0.70447 and high $^{143}Nd/^{144}Nd$ values up to 0.512667, which are consistent with a depleted within-plate mantle source. Minette and spessartite lamprophyres show high initial $^{206}Pb/^{204}Pb$, $^{207}Pb/^{204}Pb$, and $^{208}Pb/^{204}Pb$ values, whereas sannaites have lower, but variable, initial $^{206}Pb/^{204}Pb$, $^{207}Pb/^{204}Pb$, and $^{208}Pb/^{204}Pb$ values with respect to those of calc-alkaline lamprophyres. Minettes originated by partial melting of a metasomatised lithospheric mantle following siliciclastic sediment recycling by subduction. In contrast, sannaites were generated from the partial melting of a similar lithospheric mantle that was metasomatised by within-plate agents.

Key words: Alkaline and calc-alkaline lamprophyres, Geochemistry, Sr-Nd-Pb isotopes, Geochronology, Mantle heterogeneity, Iran

1. Introduction

During convergent tectonics fluids and/or melts released by partial melting of subducted sediments and/or dehydration of the oceanic slab may enrich the mantle wedge with a crustal-derived component. The delay between metasomatism and magmatism usually observed in many orogenic belts (e.g., Prelević and Seghedi, 2013 and references therein) might be some hundred million years (e.g., Wilson, 1989; Gibson et al., 1995; Tommasini et al., 2011).

The reaction between ambient peridotite of the mantle wedge with metasomatising fluids and/or melts is able to form a phlogopite- and/or amphibole-rich metasomatised vein network within the mantle wedge (e.g., Foley, 1992a, 1992b; Beccaluva et al., 2004; Conticelli et al., 2004, 2007; Bianchini et al., 2010). Partial melting of the metasomatic veins might be triggered after subduction cessation in a post-collisional geodynamic setting to produce K-rich magmas (e.g., Prelević et al., 2005; Tommasini et al., 2011).

Post collisional magmatism has been ascribed to (i) lithosphere delamination (e.g., Dewey, 1988; Turner et al., 1996, 1999); (ii) slab break-off (Davies and von Blanckenburg, 1995) and/or tearing (Prelević et al., 2012 and references therein); (iii) isotherm relaxation after subduction ending (e.g., Conticelli and Peccerillo, 1992; Conticelli et al., 2002, 2009a; Peccerillo and Martinotti, 2006; Owen, 2008) or a combination of these three scenarios.

The alkaline K-rich magmas produced in these settings are characterised by a typical arc geochemical trace element fingerprint (e.g., high large ion lithophile/high field strength element ratios; extreme enrichment in Th but with high Th/La values; e.g., Tommasini et al., 2011). Therefore, post-collisional magmatism can provide important information about the geodynamic history of the orogenic stage from oceanic subduction to continental collision and trace the evolution of the lithospheric mantle source(s).

Lamprophyres are a clan of alkaline rocks enriched in H_2O and CO_2 ranging in composition from sodic to potassic, with ultramafic to intermediate characters (Rock, 1991). Lamprophyres can be classified from alkaline and calc-alkaline, to ultramafic and lamproitic (Rock, 1991), each distinguished on the basis of their mineralogy and chemistry (Mitchell and Bergman 1991; Tappe, et al., 2005). Lamprophyric rocks with different nature are reported from different orogenic and anorogenic settings. They are reported from continental active margins (e.g., Allan and Carmichael, 1984; Lange and Carmichael, 1990; Carmichael et al., 1996), post collisional (e.g., Muller et al., 1992), late orogenic (e.g., Abdelfadil et al., 2013), intraplate rifting (e.g., Tappe et al., 2006, 2008) and intraplate basin and graben structure (e.g., Dostal and Owen, 1998). Usually, calc-alkaline lamprophyres and high-Si lamproitic lavas are considered as orogenic members of the clan. They often occur at destructive plate margins generally emplaced during post-collisional phases, although orogenic lamprophyric magmas at active continental margins are found as well (e.g., Mexico; Allan and Carmichael, 1984; Wallace and Carmichael, 1989; Lange and Carmichael, 1990; Carmichael et al., 1996). Their mineralogy and chemistry provide important information about the nature and evolution of their mantle source and geodynamic processes that might have modified it. Several models are proposed for the petrogenesis of orogenic lamprophyric magmas: (1) partial melting of metasomatic and enriched mantle (e.g., Wallace et al., 1992; Conticelli et al., 1992, 2009a; Zhang et al., 2003; Prelević et al., 2004; Owen, 2008; Avanzinelli et al., 2009); (2) contamination of mafic alkaline magmas with continental crustal material or melts (Rock, 1991; Prelević et al., 2004); (3) mixing of upwelling basaltic magma with varying amounts of ultrapotassic melts originating in the lithospheric mantle related to heating and/or thinning of sub-continental lithospheric-mantle (Thompson et al., 1990). Although lamprophyres were long thought to sample a metasomatised mantle source which has been enriched during an ancient event, it has become increasingly evident that the trace element and isotopic

signatures of already aged crust-derived material introduced during geologically young events may be an alternative explanation (e.g., Conticelli et al., 1992; Prelević et al., 2005, 2012; Tommasini et al., 2011). Geochemical and isotopic characteristics of lamprophyres confirm that both mantle and/or crustal source components may play an important role in their genesis.

Lamprophyric rocks of different nature are reported from northwestern Iran (e.g., Moayyed et al., 2008; Aghazadeh, 2009; Aghazadeh et al., 2010; Aghazadeh and Badrzadeh, 2012). They crop out as dykes and sills cutting Cretaceous and Cenozoic terranes, and they are related to the evolution of the Zagros orogen and to the subduction of Neo-Tethys ocean crust in northwestern Iran.

In this paper, we report original data on the geochronology ($^{40}Ar/^{39}Ar$ dating), petrography and mineral chemistry, whole rock geochemistry and Sr-Nd-Pb isotope composition of alkaline and calc-alkaline lamprophyres from northwestern Iran. Our aim is to shed more light on their nature and genesis and to put more constraints on the composition of the mantle wedge involved in Neo-Tethys subduction.

2. Geological background of the study area

Northwestern Iran is part of the hinterland of the Arabia–Eurasia collision zone in the broad Alpine–Himalayan orogenic belt. Mean surface elevation of the area is about 1.5–2 km above sea level with scattered Plio-Quaternary volcanoes over 3,500 meters high (e.g., Sabalan and Sahand volcanoes). The study area is located in the northwestern sector of the Zagros orogen (Fig. 1a) and it is characterised by a complex geological history, which is similar to that of the central Iranian block. The area is bounded in the east and northeast by Caspian Sea basement and lesser Caucasus ophiolite and in the west and southwest area limited by the Khoy ophiolite and Zagros suture (Fig. 1a). Two main Cenozoic magmatic arcs are found, namely the Urumieh-Dokhtar magmatic arc and the Alborz magmatic belt, which overlap partially in northwestern Iran. Magmatism started during Cretaceous times but voluminous magmatic bodies formed from late Tertiary until Quaternary (e.g., Dilek et al., 2009; Aghazadeh et al., 2011).

North-westernmost Iran, Arasbaran and southern Armenia and Nakhichevan (Azerbaijan republic) are commonly regarded as a continental terrain of Gondwanan origin (e.g.,

Berberian and King, 1981; Sosson et al., 2010 and references therein). The area includes a metamorphic basement overlain by incomplete Paleozoic terrigenous clastic and shallow marine sedimentary successions (e.g., Berberian and King, 1981; Adamia et al., 2011). Paleozoic sedimentary successions are followed by shelf marine and detrital series of Triassic to Jurassic age, with minor basic to felsic volcanic interlayers. Palaeomagnetic data from Middle Jurassic alkaline basalts and from sediments in the Nakhichevan area as well as Aalenian to Bajocian sedimentary rocks indicate a paleo-latitude of 21.5°N ± 3.7 (2000 km south of its present position) during this period of time (Bazhenov et al. 1996). Thick Cretaceous to Paleocene flysch type sediments and arc-related volcanic rocks developed in the area, especially in the Arasbaran zone, and are interpreted as being deposited in a shallow marine environment (Babakhani et al., 1990). Between the Eocene and Quaternary, syn- to post-collision magmatism (Sosson et al., 2010; Mederer et al., 2013) with typical arc geochemical characteristics was active (e.g., Dilek et al., 2009; Aghazadeh et al., 2011), representing an outstanding feature of the Arasbaran and northwestern Iran geology.

The studied lamprophyres outcrop in three areas in northwestern Iran: the Arasbaran region, the Mishu ranges, and the Eslamy (Saray) peninsula (Fig. 1b); On the basis of their mineralogy and field relationships they can be divided in two distinct groups: alkaline lamprophyres (Arasbaran range) and calc-alkaline lamprophyres (Mishu range and Eslamy Peninsula).

The Arasbaran region is mainly composed of Cretaceous to Cenozoic volcano-sedimentary successions. Amphibole-bearing (alkaline) lamprophyre outcrops as hypabyssal intrusions into the Cretaceous and Oligocene - Miocene terrains of the Arasbaran region, and they are found in the Horand and Khankandi areas (Fig. 1b). In the Horand area lamprophyres crop out in the form of sills and dykes with a NW-SE trend. They intrude flysch type sedimentary rocks and represent the oldest lamprophyric magmatic event considered (see below). The sedimentary succession is composed of sandstone, marl, and limestone of Cretaceous-Paleocene ages. A lamprophyre sill exceeds 50 m in width and 700 m in length and dykes are less than 1 m wide and 50 m length (see Appendix). In the Khankandi area several lamprophyric dykes and apophyses with NW-SE and NE-SW trends intruded in a monzonitic pluton emplaced at 28.9 Ma (Aghazadeh et al., 2010). Fragments of country monzonitic rocks are also observed in the dykes. Monzonitic pluton and lamprophyric dykes

are covered by Miocene siliciclastic sedimentary rocks. Lamprophyre outcrops are 50-200 m long and 0.5-5 m wide.

The Mishu range is delimited at both north and south edges by the northern and southern Mishu Faults (Fig. 1b). The two delimiting faults represent two branches of the Tabriz great fault (Fig. 1). Lamprophyric dykes intrude metamorphic rocks of Precambrian to Palaeozoic ages and Miocene siliciclastic sedimentary rocks. Calc-alkaline lamprophyres from Mishu range are both hornblende- and phlogopite-bearing. Hornblende-bearing lamprophyres have been found in the Sorkheh and Tasuj areas, whereas phlogopite-bearing lamprophyres are observed near the city of Marand in the Sorkheh area. Hornblende-bearing dykes cut Upper Red Formation in Sorkheh area and Precambrian metamorphic terranes in the Tasuj area. They crop out as dykes, 1-2 m wide and 300 m long. Phlogopite-bearing lamprophyres (Marand) are also found in the form of dykes with N-S to NW-SE trends, with grey colour and ranging from 0.5 to 3 m in width, and up to 500 m in length (see Appendix), and they also cut the Upper Red Formation. No temporal relationships between phlogopite-bearing and hornblende-bearing calc-alkaline lamprophyric dykes have been observed.

The Eslamy (Saray) peninsula is located in the eastern shoreline of the Urumieh Lake (Fig. 1b). The Peninsula itself formed after emergence from the lake of Eslamy stratovolcano, which is Miocene in age (from 15.7 to 6.5 Ma; Moradian Shahrbabaki, 1997; Pang et al., 2013), and was built by the piling up of alkaline lavas and pyroclastic rocks ranging in composition from basanite and leucitite to trachyte and phonolite (Moeinvaziri, 1985). Northwest-southeast trending calc-alkaline lamprophyric dykes cut the volcanic pile of the Eslamy stratovolcano, outcropping mainly in its central sector, ranging from 0.5 to 3 m in width, and from 50 to 200 m in length (see Appendix).

3. Analytical techniques

About 75 fresh samples of different lamprophyres were collected from dikes and sills from northwestern Iran. Polished thin sections of each sample were studied in detail prior to microprobe analyses. Representative minerals (amphibole, pyroxene, and mica) of different lamprophyres from selected samples were analyzed using an electron microprobe (JEOL JXA 8900RL) at the University of Mainz (Table 1 and Table E1 in the Electronic Supplementary Materials). Operating conditions include an accelerating voltage of 15 kV, a beam current of

12 nA, a beam diameter of 1-5 μm, and a peak counting time of 15-30 s. Synthetic and natural minerals were used for standardization.

Whole-rock geochemical analysis and Sr, Nd and Pb isotope determinations were performed on 27 selected samples (Table 2, Table 3 and Table E2 Electronic Supplementary Material). Major and trace elements were analysed at the ALS Analytical Laboratories Ltd. in Canada using inductively coupled plasma-emission spectrometry (ICP-ES) for major elements and inductively coupled plasma-mass spectrometry (ICP-MS) for trace elements. Major oxides were reported on a 0.2 g sample analyzed by ICP-emission spectrometry following a lithium metaborate/tetraborate fusion and dilute nitric digestion. Loss on ignition (LOI) was determined by weight difference after ignition at 1000 °C. The precision and accuracy, as indicated by duplicates and the USGS standards, are within 1% for major elements and 10% for minor and trace elements.

Sr, Nd, and Pb isotopes were analysed at the Radiogenic Isotopes Laboratory of the University of Florence. All samples were processed by sequential HF-HNO_3-HCl dissolution and the Sr, Nd and Pb fractions were purified and collected as described in Avanzinelli et al. (2005). Sr-Nd-Pb isotope ratios were measured with a Thermal Ionisation Mass Spectrometer (TIMS) ThermoFinnigan Triton-Ti®. During the period of measurement the mean value for $^{87}Sr/^{86}Sr$ of the NIST SRM 987 standard was 0.710249±15 (2σ, *n=17*), and the mean values for $^{143}Nd/^{144}Nd$ of the NdFi and La Jolla standards were 0.511471±6 (2σ, *n=12*) and 0.511846±7 (2σ, *n=67*) respectively (further details are reported in Electronic Supplementary Material). Mass fractionation of Sr and Nd isotopes has been exponentially corrected to $^{86}Sr/^{88}Sr$ =0.1194 and $^{146}Nd/^{144}Nd$ = 0.7219, respectively. Pb isotope ratios were corrected for instrumental mass bias using replicate analyses of NIST SRM 981 standard. The long term and within run averages for $^{206}Pb/^{204}Pb$, $^{207}Pb/^{204}Pb$ and $^{208}Pb/^{204}Pb$ are also reported as Electronic Supplementary Material. Mass bias during Pb isotope analysis was monitored with repeated measurements of SRM 981 reference sample with an average fractionation factor of 0.149 % per mass unit relative to the reference values (Thirlwall, 2000) that was applied to all Pb isotope ratios. The accuracy of Pb isotope data was further tested by replicate measurements of AGV-1 yielding averages of $^{206}Pb/^{204}Pb$ 18.940±0.014 (2σ, *n=11*), $^{207}Pb/^{204}Pb$ 15.653±0.017 (2σ, *n=11*), $^{208}Pb/^{204}Pb$ 38.566±0.061 (2σ, *n=11*), which are within the error of the values reported by Weis et al. (2006); analytical details are provided in Avanzinelli et al. (2005).

$^{40}Ar/^{39}Ar$ incremental heating experiments were conducted on 4 samples of phlogopite and amphibole crystals, separates by hand-picking method, from MA-01, SA-03, MA-08 and HO-03 samples (Table E3 Electronic Supplementary Material) After crushing and sieving, the crystals were hand-picked from the 100-300 µm size fraction. Resulting mineral separates and chips were cleaned using an ultrasonic disintegrator. Minerals were then etched in 15 vol.% hydrofluoric acid for 10 min. Samples were neutron irradiated at the 5 MW reactor of the GKSS Reactor Center (Geesthacht, Federal Republic of Germany), with crystals and matrix chips in aluminium trays and irradiation cans wrapped in 0·7 mm cadmium foil. Samples were step-heated by laser. Purified gas samples were analyzed using a MAP 216 noble gas mass spectrometer. Raw mass spectrometer peaks were corrected for mass discrimination, background and blank values determined every analysis. The neutron flux was monitored using TCR sanidine (Taylor Creek Rhyolite = 27·92 Ma; Dalrymple and Duffield (1988)) and internal standard SAN6165 (0·470 Ma; Van den Bogaard, 1995). Vertical variations in J values were quantified by a cosine function fit. Lateral variations in J were not detected. Corrections for interfering neutron reactions on Ca and K are based on analyses of optical grade CaF_2 and high-purity K_2SO_4 salt crystals that were irradiated together with the samples. Ages derived from step-heating analyses are based on plateau portions of the age spectra. Plateau regions generally comprise > 50% of the ^{39}Ar released and more than three consecutive heating steps that yield the same ages (within 2 S.D.).

4. Petrography, classification, and mineral chemistry

The studied rocks show all major petrographic characteristics generally accepted by earlier definitions of lamprophyres (e.g., Wimmenauer, 1973; Rock, 1977, 1991; Streckeisen, 1978; Le Maitre et al., 2000). According to them, lamprophyres are melanocratic hypabyssal igneous rocks with microporphyritic textures carrying hydrous mafic phenocrysts. Feldspars and other felsic minerals are always restricted to the groundmass. The high modal phenocryst contents comprised of hydrous mafic minerals (typically amphibole and phlogopite) indicates a primary hydrous nature of the parental, mantle-derived lamprophyric melts (Rock, 1991).

4.1 Petrography and Classification

4.1.1 Arasbaran alkaline lamprophyres

Horand lamprophyres are dark grey to green in colour with porphyritic textures. They are characterised by the occurrence of amphibole phenocrysts to megacrysts, which in some cases are longer than two cm, set in a groundmass made up dominantly by alkali-feldspar. Microscopically the amphibole-bearing lamprophyres show porphyritic and panidiomorphic texture (Fig. 2a). Amphibole also occurs in the groundmass along with clinopyroxene, K-feldspar, plagioclase, mica, and opaque minerals. Apatite and zircon occur as accessory minerals.

Khankandi alkaline lamprophyres are also amphibole-bearing with similar texture and mineralogy to the *Horand* ones. Amphibole-bearing lamprophyres have mafic minerals and feldspars (i.e., plagioclase and K-feldspar) in the groundmass that are replaced by chlorite, calcite and sometimes sericite, serpentine, clay minerals and zeolites (Fig. 2b).

According to their mineralogy the *Arasbaran alkaline lamprophyres* from the Horand and Khankandi areas (Fig. 1b) are classified, respectively, as sannaite and camptonite alkaline lamprophyres (Le Maitre et al., 2002). These lamprophyres might have contained feldspathoids that are not observed in the studied samples due to the strong alteration of the groundmass. Normative *nepheline*, however, does occur in the CIPW norm of the amphibole-bearing lamprophyres (Horand 5.6 mol.% < *ne* < 1.8 mol.%; Khankandi 6.5 mol.% < *ne* < 0.2 mol.%; Table 2).

4.1.2 Mishu and Eslamy calc-alkaline lamprophyres

Mishu (Sorkheh and Tasuj) lamprophyres are hornblende-bearing with similar texture and mineralogy to the alkaline ones of *Horand* and *Khankandi. Mishu lamprophyres* display also the occurrence of olivine ghosts (Fig. 2c), with, in some cases, coronas made by clinopyroxene. They have a relatively high abundance of plagioclase with respect to K-feldspar in the groundmass and are classified as spessartite.

Phlogopite-bearing lamprophyres from Eslamy and Marand areas are characterised by 30-40 vol.% of large fresh phlogopite crystals, which may be up to 5 cm in diameter (Fig. 2d), set in a groundmass made of phlogopite, clinopyroxene, K-feldspar, plagioclase, and opaque minerals. They have porphyritic texture (Fig. 2d) with phenocrysts of phlogopite and clinopyroxene. Mica crystals show pale brown cores and dark brown margins. Clinopyroxene phenocrysts are euhedral, sometimes replaced by calcite, chlorite and opaque minerals.

Accessory minerals are dominantly apatite and opaque minerals. Chlorite, calcite and zeolite are abundant in the matrix.

Phlogopite-bearing lamprophyres (Table 2) are classified as minette (Le Maitre, 2002), although chemical differences between minette from Eslamy and those from Marand do exists (Fig. 3a). Indeed, the minette at Eslamy shows the highest alkali contents, which are coupled with the highest K_2O and the highest, and largely variable, K_2O/Na_2O ratios (i.e., 3.9-13.4). The Eslamy minettes also show the occurrence of *leucite* in their CIPW norm ($3.7 < lc < 21.8$), which is not observed in any other studied rocks (Table 2). Eslamy minettes are the only one that may be classified as ultrapotassic (Foley et al., 1987) (MgO > 3 wt.%, $K_2O/Na_2O > 2$ and K_2O > 3 wt.%; Table 2), with the highest K_2O/Na_2O values. In the CaO versus Al_2O_3 diagram (Fig. 3b) presented for ultrapotassic rocks (Foley et al., 1987), the Eslamy minettes fall within the Roman province field, Italy, although they do not contain leucite.

4.2 Mineral chemistry

Clinopyroxene from sannaites and camptonites (e.g., Khankandi and Horand lamprophyres) is diopside to salite in composition ($Wo_{45-50}En_{28-44}Fs_{7-21}$; Table 1). Clinopyroxene from minette and spessartite (e.g., Eslamy and Mishu lamprophyres) ranges from diopside-salite to augite ($Wo_{40-49}En_{35-49}Fs_{3-19}$; Table 1). Clinopyroxene shows normal compositional zonation from core to rim, with cores enriched in diopside component with a rimward enrichment in hedenbergite component. When compared to each other clinopyroxene from alkaline lamprophyres and calc-alkaline lamprophyres show clear differences in terms of Mg#, Al_2O_3 and TiO_2 (Table 1). Clinopyroxene from sannaite-camptonites show higher Al_2O_3 and TiO_2 (Fig. 4a) and lower Mg-# [Mg/(Mg+Fe)] and SiO_2 contents, than clinopyroxene in minettes and spessartite (Table 1). The most distinctive difference between the two groups is observed in the Na_2O content with the clinopyroxene from Khankandi camptonite showing the highest Na_2O content (up to 1.17 wt. %; Table 1).

Brown mica has a phlogopite composition with high Mg# [Mg/(Mg+Fe)> 0.79] decreasing rimward (Fig. 4b; Table 1). As a corollary, phlogopite shows normal zoning, especially in the Eslamy minette, with increasing annite end member from core to rim (Table 1). Phlogopite in the Eslamy minette has lower Al_2O_3 and Na_2O and higher MgO and SiO_2 contents than mica in Marand minette (Table 1). Compositional variations in micas follow two distinct arrays: (i) the phlogopite from the Marand minette follows the lamprophyric array (i.e. shoshonitic nature)

on the plot of Al_2O_3 vs. TiO_2 (Fig. 4c) and FeO (not shown); (ii) Eslamy minette phlogopite follows the lamproitic array (Mitchell and Bergman, 1991). Relative to Mediterranean minettes and lamproites, micas in the studied minettes show higher Al_2O_3 but lower SiO_2 (Fig. 4b, 4c and Table 1). From this point of view, micas in Eslamy peninsula minettes are more similar to those in Mediterranean lamproites (Fig. 4b, 4c).

Amphibole from alkaline lamprophyres (i.e., camptonite and sannaite) has calcic-kaersutitic composition, whereas the few analyzed crystals from calc-alkaline lamprophyres (i.e., spessartite) have magnesio-hastingsite and hastingsite compositions. The TiO_2 content in most amphibole crystals of alkaline lamprophyres is higher than 5 wt.% in keeping with the within plate alkaline nature of the magmas from which they crystallise (Fig. 4d). Amphibole from the Horand sannaite shows lower Mg# at comparable silica content than that from Khankandi camptonite (Table 1).

5. $^{40}Ar/^{39}Ar$ dating

The Ar isotope data and measured K_2O concentrations for mica and amphibole separates from 4 different alkaline and calc-alkaline samples are listed in Table E3 (electronic supplementary materials) and the $^{40}Ar/^{39}Ar$ age spectra are presented in the figure 5. Amphibole crystals separated from Horand (*Arasbaran alkaline lamprohyres*) sannaite samples yield weighted mean plateau dates of 81.2 ± 1.8 Ma (95% conf. MSWD = 129) and 81.4 ± 1.4 Ma (95% conf. MSWD = 72). Amphiboles separated from Sorkheh (*Mishu calc-alkaline lamprohyres*) spessartite samples yield weighted mean plateau ages of 9.57 ± 0.25 Ma (2σ, MSWD = 2.7) and 9.95 ± 0.11 Ma (2σ, MSWD = 2.0). Separated mica from Marand (*Mishu*) and Eslamy minettes yield 10.98 ± 0.04 Ma (2σ, MSWD = 0.53) and 10.35 ± 0.02 Ma (2σ, MSWD = 2.5), respectively (Fig. 5 and Table 3).

The Horand sannaites are the oldest dated lamprophyres in the area and their emplacement age is Late Cretaceous (Campanian). Our $^{40}Ar/^{39}Ar$ age data are in accordance with the field observations showing that these lamprophyres metamorphosed the Cretaceous sedimentary strata. On the other hand, the Khankandi camptonite dykes have not been dated, but we suppose an age range between 28 and 15 Ma because they cut the 28 Ma Khankandi monzonitic intrusion (Aghazadeh et al., 2010), but not the overlaying Miocene sedimentary rocks.

6. Whole rock chemistry and radiogenic isotopes

The studied lamprophyres show variable SiO_2 contents: 40-46 wt. % for the Arasbaran camptonites and sannaites (alkaline lamprophyres), 44-48 wt.% for the Sorkheh (Mishu calc-alkaline lamprohyres), and 42-48 wt. % for the Marand (Mishu calc-alkaline lamprohyres) and Eslamy minettes (calc-alkaline lamprohyres) (Table 2). Sannaites and camptonites are generally enriched in TiO_2 with values higher than 1.6 wt.%, whereas spessartites and minettes show values lower than 1.7 wt.%. Sannaites and camptonites show high and variable MgO (4.8-9.6 wt.%) and Fe_2O_{3t} (8.2-15.8 wt.%), whereas in calc-alkaline lamprophyres these oxides mainly range from 4.0 to 7.3 wt.% and from 8.4 to 12 wt.%, respectively (Table 2). Minettes are enriched in K_2O, ranging from 4.6 to 8.1 wt.% for the Eslamy, whereas in sannaites and camptonites K_2O is lower than 4.1 wt.% (Table 2). Most of the studied rocks are MgO-rich (Table 2) and MgO content decreases with increasing silica. Phosphorus (P_2O_5) in minettes is in the range between 0.64 and 1.43 wt.% partially overlapping the range shown in sannaites and camptonites (0.46-1.48 wt.%), although some higher values are observed in spessartites (P_2O_5 = 0.71-1.94 wt.%). Overall, the lamprophyres have high L.O.I. (2.6-7.1 wt.% in camptonite; 1.4-2.7 wt.% in spessartite; 3.8-7.7 wt.% in minettes), with the highest values found in the most weathered rocks characterised by carbonate-rich secondary minerals.

Regarding compatible trace elements, Ni and Cr show largely variable compositional ranges from 10 to 230 ppm and from 30 to 300 ppm, respectively in sannaites and camptonites, and from 21 to 86 ppm and 50 to 138 ppm in minettes. Minettes show the strongest enrichment in LILE and depletion in HFSE (Nb, Ta, Ti), with positive spikes at Pb and P in the incompatible patterns normalised to primitive mantle (Fig. 6a). Similar plots for sannaite and camptonite samples do not show any fractionation between LIL and HFS elements, with patterns showing typical positive spikes at Ti, and negative ones at Pb (Fig. 6b). Spessartite calc-alkaline lamprophyres from Sorkheh and Tasuj (Mishu) show distinct patterns with P and Ti positive spikes and mild negative anomalies in Nb-Ta and Pb (Fig. 6c), showing intermediate patterns between alkaline lamprophyres and minettes.

Sr, Nd and Pb isotope data are reported in the Table 3. Initial isotope ratios are calculated for the individual $^{40}Ar/^{39}Ar$ radiometric ages (Table E2 in the electronic supplementary materials) and the inferred range of ages for the samples from Khankandi camptonite dykes. Two groups are readily distinguishable: the late Cretaceous sannaites on one side (alkaline

lamprophyres), and the Miocene Eslamy minettes, on the other one. Alkaline lamprophyres are characterized by consistently low initial $^{87}Sr/^{86}Sr$ (0.70447-0.70563) and high $^{143}Nd/^{144}Nd$ (clustering 0.51267) values, whereas Eslamy minettes show the highest initial $^{87}Sr/^{86}Sr$ (0.70752-0.70760) and the lowest initial $^{143}Nd/^{144}Nd$ (0.51246-0.51247) values. Spessartite calc-alkaline lamprophyres show initial $^{87}Sr/^{86}Sr$ (0.70476-0.70568) and initial $^{143}Nd/^{144}Nd$ (0.51267-0.51275) values overlapping those of Arasbaran lamprophyres within error (Fig. 7), whilst minette from Marand has slightly lower initial $^{87}Sr/^{86}Sr$ (0.70737-0.70740) and higher initial $^{143}Nd/^{144}Nd$ (0.51256-0.51258) relative to Eslamy. Minettes from northwestern Iran (e.g., Eslamy and Marand) overlap the Sr-Nd isotopic field of Miocene lamproite from Corsica (Sisco; Conticelli et al., 2007, 2009b; Prelević et al., 2010). Cretaceous sannaites and camptonites (e.g., Horand and Khankandi) show initial Sr and Nd isotopic values overlapping the isotopic composition of Oligocene to Eocene within-plate basalts and lamprophyres from the Central Mediterranean (e.g., Avanzinelli et al., 2012a, 2013), and fall well within the field of CiMACI (Circum Mediterranean Anorogenic Cenozoic Igneous) province (Lustrino and Wilson, 2007). Spessartite lamprophyres of Miocene age from Iran (i.e., Sorkheh) also overlap the isotopic composition of CiMACI field (Fig. 7).

Lead isotopes show great variability with Arasbaran lamprophyres showing large ranges in initial $^{206}Pb/^{204}Pb$ (18.448-18.920), $^{207}Pb/^{204}Pb$ (15.609-15.617), and $^{208}Pb/^{204}Pb$ (38.783-39.025) ratios, overlapping completely with the lead isotope ratios of spessartite from Sorkheh and Tasuj ($^{206}Pb/^{204}Pb_i$ = 18.821-18.973; $^{207}Pb/^{204}Pb_i$ = 15.644-15.667; $^{208}Pb/^{204}Pb_i$ = 38.923-39.069). Eslamy minettes show the highest lead isotopic ratios ($^{206}Pb/^{204}Pb_i$ = 19.015-19.099; $^{207}Pb/^{204}Pb_i$ = 15.669-15.689; $^{208}Pb/^{204}Pb_i$ = 39.159-39.246). The Pb isotopic ratios of minettes differ from those of Mediterranean lamproites and lamprophyres (e.g., Conticelli et al., 2002, 2009b; Owen, 2008; Prelević et al., 2008, 2010), having slightly higher $^{206}Pb/^{204}Pb_i$ values. All samples plot above the terrestrial mantle array and the Northern Hemisphere Reference Line (NHRL) (Hart, 1984) on $^{207}Pb/^{204}Pb$ vs. $^{206}Pb/^{204}Pb$ and $^{208}Pb/^{204}Pb$ vs. $^{206}Pb/^{204}Pb$ (Fig. 8a, 8b).

7. Discussion

The Iranian lamprophyres cover a wide chronological range, from Cretaceous to Miocene, covering the last stage of the Tethys closure from active continental margin until continental collision. The oldest magmatic events are represented by the Horand sannaites intruded at

between 81.2-81.4 Ma (Fig. 5) and they show a clear within-plate signature (Fig. 6b). The same holds true for the Khankandi camptonites intruded close in space to the Horand alkaline lamprophyres, in the Arasbaran region (Fig. 1b), between 28 and 15 Ma and still have a clear within-plate signature.

The intrusion age of spessartite lamprophyres and their peculiar mineralogy and chemistry give more significance to this magmatism. They are Miocene in age and almost coeval with the minettes of the Marand and Eslamy nearby areas (Fig. 1b). Indeed spessartite lamprophyres were intruded between 9.57 ± 0.25 and 9.95 ± 0.11 Ma after the emplacement of the Marand (10.98±0.04 Ma) and Eslamy (10.35 ± 0.02 Ma) minettes. Marand and Eslamy minettes display clear subduction-related trace element patterns (Fig. 6a), whilst spessartite lamprophyres show both subduction-related and within-plate characteristics, with mild negative anomalies at Ta and Nb and negative spike at Pb, and a positive one at Ti (Fig. 6c). The occurrence of lamprophyres with such contrasting signature is intriguing and their study might shed some further light on the geodynamic processes related with the closure of the Tethys in the northwestern Iran, Caucasus and surrounding regions.

7.1 Alteration and low-pressure crustal contamination

Given the fact that lamprophyres usually represent magma batches of small volumes intruded in a dynamic tectonic setting, either secondary alteration or low-pressure crustal contamination might have played a role in the acquisition of final geochemical and isotopic signatures (Rock, 1991). Before discussing the magma genesis and mantle source characteristics, possible effects related to low pressure processes need to be investigated in some detail.

The lamprophyres show a wide range of loss on ignition (LOI), from 1.5 wt.% to about 8 wt.% (Table 2). Minette samples are characterised by extremely high LOI values up to 8 wt.%, which cannot be due to high phlogopite contents. Due to its crystal chemistry, phlogopite can accommodate not more than 4 wt.% of OH, F and/or Cl, which indicate that > 2-3 wt.% of the LOI is due to weathering or related to either crystallisation of secondary calcite or alteration of glass within the groundmass. Alteration did not greatly influence other geochemical parameters like the contents of LILE and isotopic compositions, as demonstrated by the relatively constant $^{87}Sr/^{86}Sr$ values, K_2O and Rb contents for samples with extremely variable LOI and similar degree of differentiation. Conversely, LOI in Horand sannaites and Sorkheh

and Tasuj spessartite clearly correlates with $^{87}Sr/^{86}Sr$ values, K_2O and Rb contents (Fig. 9) indicating that the extensive post-emplacement weathering might have affected their compositions. The variation observed in the initial $^{87}Sr/^{86}Sr$ at constant initial $^{143}Nd/^{144}Nd$ (Fig. 7) are strongly suggestive of addition of fluids derived from continental crustal rocks during post-emplacement processes (Staudigel et al., 1995).

On the other hand, crustal contamination might have played an important role in genesis of lamprophyres. Indeed incompatible trace element enrichment with fractionated HFSE with respect to LILE is a geochemical characteristic typical of the upper continental crust (e.g., Taylor and McLennan, 1985; Elliot et al., 1997; Plank and Langmuir, 1998; Plank, 2005; Conticelli et al., 2007, 2009a; Avanzinelli et al., 2012b). When small batches of magma penetrate thick continental crust, such as that of an active continental margin, crustal contamination might occur (DePaolo, 1981). Shallow level crustal contamination is able to increase initial $^{87}Sr/^{86}Sr$ and concomitantly decrease initial $^{143}Nd/^{144}Nd$. However, to obtain the increase of incompatible trace elements at the levels observed in the high-Mg rocks studied here, a large amount of assimilated crust is needed, which would result in dramatic decrease in the MgO and compatible trace element contents (e.g. Conticelli, 1998; Murphy et al., 2002).

Marand and Eslamy minettes show the highest initial $^{87}Sr/^{86}Sr$ and the lowest initial $^{143}Nd/^{144}Nd$ of the entire set of studied samples (Fig. 7), with the strongest fractionation HFSE with respect to LILE (Fig 6a-6c) and normalised incompatible trace element patterns resembling those of GLOSS and Mediterranean potassic rocks (Fig. 6d). In figure 10 the variation of initial $^{87}Sr/^{86}Sr$ vs. MgO of the studied rocks is shown, and two distinct arrays can be clearly observed: (i) the minette array at high and constant initial $^{87}Sr/^{86}Sr$ and variable MgO; (ii) the Horand sannaite and the Sorkheh and Tasuj spessartite array at low initial $^{87}Sr/^{86}Sr$ and variable MgO showing a clear negative correlation. These geochemical characteristics clearly indicate that: (i) minettes and camptonites are from different parental magmas; (ii) minette undergoes neither simple crustal contamination nor AFC processes; (iii) Horand camptonites and the intermediate lamprophyres did undergo some crustal contamination during differentiation.

In summary, on the basis of petrographic and geochemical data we may argue that the most primitive rocks of the camptonite and minette series are mantle derived magmas that

underwent some extent of low-pressure differentiation processes plus alteration, but the isotopic and trace element ratios of the MgO-rich samples can be considered as primary characteristics acquired from their mantle sources during partial melting.

7.2 Enrichment of lamprophyric mantle source: two types of mantle metasomatism

Lamprophyric magmas in northwestern Iran occurred in three different periods with different mineralogical, geochemical and isotopic characteristics. The major issue here is to constrain whether these different lamprophyric types are derived from asthenospheric or lithospheric mantle. For the ultrapotassic calc-alkaline lamprophyres (i.e., minettes from Eslamy and Marand) their high abundances of MgO and Ni with respect to FeO, Na_2O, and Cr are strongly suggestive for a lithospheric mantle source. However, the high K and large ion lithophile incompatible trace elements contents suggest that the lithospheric mantle source was newly fertilised via metasomatism by volatile-rich melts prior to partial melting (e.g., Foley, 1992a; Tappe et al., 2007, 2008). Furthermore, lithospheric mantle is a viable source also for the alkaline lamprophyres, and this is based mostly on their Sr, Nd and Pb isotopic signature that are considerably more “enriched” relative to the convecting mantle array illustrated by MORB or OIB fields (Fig. 7 and Fig. 8).

7.2.1. Mantle source of sannaite and camptonite magmas

Sannaite and camptonite lamprophyres from Arasbaran region show lower Mg-# and Ni and Cr in comparison to primary basaltic magmas originated from fertile mantle sources (Frey et al., 1978), and so represent differentiated magmas from mantle-derived primary melts. Clinopyroxene in the sannaite and camptonite shows Al_2O_3 and TiO_2 compositions higher than in the sub-alkaline or tholeiitic basalts. High TiO_2 and Fe_2O_3 content of sannaite and camptonite lamprophyres are similar to experimental melts produced by partial melting of a fertile peridotite (e.g., Falloon et al., 1988). Their enrichment in incompatible trace elements, considerably more than observed in the OIBs, clearly indicates metasomatism of their mantle source. This is further supported by "enriched" Sr, Nd and Pb isotopic signatures, which are outside of those typical of MORB and OIB magmas (Fig. 7 and Fig. 8).

The sannaites and camptonites have high and smooth REE patterns and incompatible trace element patterns (Fig. 6b) with negative Pb anomalies typical of ocean island basalts

(e.g., Edwards et al., 1994; Hofmann 1997). Furthermore, they have initial $^{143}Nd/^{144}Nd$ and $^{87}Sr/^{86}Sr$ composition falling in the upper left quadrant of the plot of Figure 7. The 80 Ma old Horand sannaites show a wide range of $^{206}Pb/^{204}Pb$ and $^{208}Pb/^{204}Pb$ ratios and higher $^{207}Pb/^{204}Pb$ relative to Khankandi younger camptonite (Table 3; Fig. 8). In order to test if a crustal component was involved in the petrogenesis of the amphibole lamprophyre, we used a Th/La ratio that is considered as a canonical trace element ratio (Hofmann and White, 1982) and is very sensitive to trace the involvement of the upper crust either as a low pressure contaminant during assimilation (Sun and McDonough, 1989) or a tracer for upper crust recycling into the upper mantle (e.g., Plank, 2005; Tommasini et al., 2011). Arasbaran alkaline lamprophyres show Th/La between 0.05 and 0.19, with Khankandi camptonite at the lower end (0.05-0.08) and Horand sannaite at the upper one (0.12-0.19), with values comparable to those of the primitive mantle (~0.12, Sun and McDonough, 1989). On the other hand, Eslamy and Marand minettes have higher Th/La values that fall well within the field of arc magmas defined by Plank (2005) with the Eslamy minette overlapping the value of the upper crust (i.e., Rudnick and Gao, 2003), at the low Th/La end of the Tethyan Realm lamproites (Fig. 11) (Tommasini et al., 2011).

In the Arasbaran alkaline lamprophyres the Th/U (45-199), Nb/U (28-62), Ba/Nb (2.4-4.2), Ce/Pb (0.06-0.13) and Th/Nb (12-13) ratios (e.g., Taylor and McLennan, 1985) are comparable with typical oceanic within plate basalts (OIB) arguing for a within plate mantle source for sannaitic and camptonitic magmas. These criteria can be well seen in the Th/Nb vs. $^{87}Sr/^{86}Sr$ plot (Fig. 12) where the Arasbaran alkaline lamprophyres and Sorkheh and Tasuj spessartites fall well within the OIB field. In contrast, Eslamy minettes overlap with the upper crustal Th/Nb value and the Marand minette is close to it (Fig. 12). The Th/Yb versus Nb/Yb plot is used to confirm these findings (Pearce, 2008), showing a mantle array characterised by mean OIB, E-MORB, N-MORB with subduction-related volcanic rocks falling at higher Th/Yb ratios than those of the mantle array (Fig. 13). In this plot the Arasbaran alkaline lamprophyres fall in mantle array at its OIB end, with Khankandi and mafic Horand samples falling in the middle of the array with the most evolved ones straddling the boundary of the mantle array (Fig. 13). Eslamy and Marand minettes plot at higher Th/Yb values well within the field of active continental margins, defining a linear array parallel to the MORB-OIB oceanic array (Fig. 13). It is important to note the position of the Sorkheh and Tasuj spessartites at higher Th/Yb and

variable Nb/Yb values describing a mixing array between the Eslamy minette and the MORB-OIB array (Fig. 13). This suggests that their parental magmas were probably generated by mixing between calc-alkaline and within-plate magmas.

Volatile-bearing minerals such as phlogopite and amphibole are the major mineral repositories for LILE in lithospheric mantle (Foley et al., 1996). Melts produced by the melting of amphibole-bearing peridotite are expected to have low Rb/Sr (<0.1) and high Ba/Rb (>20) whereas melts produced by melting of phlogopite-bearing assemblages are expected to have higher Rb/Sr (>0.1) and lower Ba/Rb (<20) (Furman and Graham, 1999). In both cases, hydrous phases are expected to dominate the contribution to the melting assemblages (e.g., Foley et al., 1999; Conceição, and Green, 2004; Pilet et al., 2005, 2008). Arasbaran alkaline lamprophyres and Sorkheh and Tasuj spessartite show very low Rb/Sr (0.02-0.1) indicating the occurrence of amphibole as a major metasomatic phase in the mineralogy of their sources. The low Ba/Rb ratio (11-21) found in sannaite and camptonite argues against the occurrence of K-richterite suggesting either pargasitic or kaersutitic amphibole as repository of the metasomatic within-plate component in their mantle source (Tiepolo et al., 2002). Minette samples have higher Rb/Sr (0.09-0.36, except one sample 0.06) and lower Ba/Rb (8-21, except one sample 27.2) indicating a predominance of phlogopite rather than amphibole in the mantle source.

Arasbaran amphibole-bearing lamprophyres (i.e., sannaites and camptonites) show OIB-type geochemical signature, although their LILE (e.g. K, Rb, Sr) and LREE contents are two or three times higher than typical OIB type magmas (e.g., Sun and McDonough, 1989; Table 2). In addition, amphibole-bearing Arasbaran lamprophyres display low Ba/Rb ratios suggesting the possible occurrence of either pargasitic or kaersutitic amphibole in their mantle source. Amphibole is unstable in the asthenospheric mantle and in uprising deep mantle plumes, whilst it can crystalize in lithospheric upper mantle due to interaction with metasomatic agents derived from convecting mantle regions (Class and Goldstein, 1997). Therefore, Arasbaran amphibole-bearing parental magmas might have been produced by partial melting of lithospheric upper mantle in a within-plate tectonic regime. The La/Nb ratio and La concentrations can separate subduction-modified asthenospheric sources from lithospheric mantle metasomatised via asthenosphere-derived melts (Seghedi et al., 2004). Arasbaran amphibole bearing lamprophyres show low La/Nb ratios (almost <1) and high La content

(almost >50). Therefore, we propose that sannaitic and camptonitic magmas originated from metasomatised lithosphere that was enriched by asthenosphere-derived melts during Cretaceous (Horand) and Oligo-Miocene (Khankandi) times.

7.2.2. Marand and Eslamy minettes mantle source: Recycling of Upper Crust into the lithospheric mantle

Eslamy and Marand minette have geochemical and mineralogical characteristics clearly indicating an ultimate derivation from the mantle (e.g., olivine on liquidus, high Ni and Cr, high MgO). However, their isotopic and REE signatures, including enrichment in LILE and radiogenic isotopic data, are close to upper crustal values. Enrichment in LILE and radiogenic isotopes cannot be explained by crustal contamination whereas the high contents of compatible elements and MgO as well as low SiO_2 content (< 48 wt.%) cannot be justified by either bulk contamination or AFC. In addition, Eslamy minettes have constant radiogenic Sr isotopic ratios with variable MgO contents and LILE enrichment associated with low Ce/Pb ratio. They have a trace element pattern suggesting involvement of crustal material in their mantle source, among which Cs, Th, U, Sr, Pb, Ba, and Rb enrichment, higher Th/La ratio as well as lower Sm/La ratio can be noticed. Particularly the strong positive spike at Pb is clearly distinctive of a recent addition of a crustal component (Fig. 6d; Taylor and McLennan, 1985). Furthermore, the following ratios signify continental crust signature in their mantle source including enrichment in Rb, Ba, Pb, Sr, U, Th, and Cs and high Th/La as well as low Sm/La. Moreover, Th/U (2.7-3.7), Nb/U (3.2-7.6), Ba/Nb (11-44), Ce/Pb (1.1-6.9) and Th/Nb (0.49-0.99) ratios indicate continental crust signature (e.g., Taylor and McLennan, 1985). All the above reported characteristics argue for a recycling of sediments within the upper mantle during subduction (e.g., Elliot et al., 1997; Avanzinelli et al., 2012a; Prelević and Seghedi, 2013). Partial melting of sediments provides metasomatic agents (melts and/or fluids) that react with the ambient lithospheric mantle source to stabilise a new mineralogy with a dominance of phlogopite and/or K-richterite.

7.2.3. Sorkheh and Tasuj spessartite: melting of heterogeneous mantle source

Hornblende-bearing lamprophyres of the Sorkheh and Tasuj areas (spessartite) have distinctive mineralogical, geochemical and isotopic characteristics from both alkaline lamprophyres and minette in that they have amphibole and clinopyroxene as the main mafic

minerals. According to clinopyroxene chemistry they are comparable with minette type lamprophyres. Geochemically, they have similar features to minette type lamprophyres. They demonstrate important negative Nb-Ta anomalies like mica-lamprophyres as well, but they have positive Ti, P and negative Pb anomalies, which makes them comparable to camptonite and sannaite lamprophyres. It is noteworthy that they do not show typical enrichment in LILE as in minette type lamprophyres. However, they are similar to minette in that they show positive K anomalies in their trace element patterns while no such positive peak in camptonite and sannaite is observed. Their Sr and Nd isotopic ratios are similar to Horand and Khankandi camptonite and sannaite type lamprophyres and located in the depleted quadrant near the bulk earth (Fig. 7).

In the Th/Yb versus Nb/Yb diagram the intermediate lamprophyres fall outside the mantle array and plot between the mantle array and the active continental margin field. This may indicate that the parental magma of the intermediate lamprophyres originated from a mixed source. The source included two types of metasomatism - one that was tapped by minette melts and the other one similar to the within-plate mantle source of the older sannaitic to camptonitic magmas. The occurrence of olivine on the liquidus in the intermediate lamprophyres and their mafic chemistry preclude the possibility that they originated by crustal contamination.

7.3 Geodynamic implications

The studied area is part of the Zagros orogen that includes magmatism related to the subduction of Neo-Tethys oceanic crust during Cretaceous-Late Eocene time and post collisional magmatism during and after collision between Arabian and Eurasian continents from Late Eocene time onwards (e.g. Allen and Armstrang 2008; Aghazadeh et al., 2011). Several terranes separated from Gondwana and collided with Eurasia during Late Paleozoic to Early Cenozoic time (Stampfli and Borel, 2002). During Late Triassic-Early Cretaceous time Central Iran collided with Eurasia and northeastward subduction of the Neotethys oceanic crust beneath the Eurasian margin caused continuous active arc magmatism along the Lesser Caucasus and Sanandaj–Sirjan Zone (Sosson et al., 2010; Agard et al., 2011 and references therein). In northwestern Iran two branches of the Neo-Tethys ocean were active and include the Khoy branches in the south (Khalatbari-Jafari et al., 2006) and lesser Caucasus branch in

the north (Rolland et al., 2007; Galoyan et al., 2009) (Fig.1). During Jurassic-Cretaceous time duplicate subduction of these branches caused two magmatic arcs to develop in northwestern Iran and Lesser Caucasus, respectively (Sosson et al., 2010). Magmatic rocks related to these volcanic arcs with typical arc signatures are exposed in the western part of NW Iran that can be regarded as the NW continuation of the Sanandaj-Sirjan zone (e.g. Azizi and Jahangiri, 2008; Ghalamghash et al., 2009; Azizi et al., 2014) and lesser Caucasus and southern Armenia (e.g. Roland et al., 2009; Mederer et al., 2013). The northern oceanic branch closed during Late Cretaceous-Palaeocene time and the South Armenian block and Arasbaran zone collided with Eurasia (Sosson et al., 2010). However, the southern branch closed in the Paleogene, connecting northwestern Iran and Arabian plates (Allen and Armstrang, 2008; Aghazadeh et al., 2011). During Paleogene collision, the Arasbaran and South Armenian blocks experienced uplifting and formation of foreland basin and folding as a passive margin of northern oceanic branch (Sosson et al., 2010). In the Arasbaran area Cretaceous volcanic rocks followed by flysch type sedimentation with volcanic interlayers represent the latest existence of an arc in the area. Extensive magmatism in this area during the Eocene to Miocene is ascribed to a collisional context (Sosson et al., 2010; Aghazadeh et al., 2011).

Lamprophyric magmatism in northwestern Iran was active from late Cretaceous to late Miocene time. Alkaline, amphibole-bearing lamprophyric magmatism occurred in different tectonic episodes in late Cretaceous, late Oligocene and late Miocene times. The oldest alkaline lamprophyres (Horand and Khankandi sannaites and camptonites) originated from metasomatised lithosphere that was enriched by deep asthenosphere-derived melts. Sannaitic to camptonitic lamprophyric magmatism taps heterogeneously metasomatised lithospheric mantle that melted due to tectonic instability. The Late Cretaceous geological situation in the area most likely suggests late stage development of the volcanic arc, meaning that the oceanic basin had just closed (flysch sedimentation). This is also supported by the fact that the lamprophyres cut flysch sediments. If this is true, then the lamprophyric magmatism might represent the waning stage of the subduction-related tectonics, and the initiation of collisional/postcollisional tectonics. A potential trigger of mantle melting might be slab breakoff (Davies and von Blanckenburg, 1995) or slab tear. In that case, precursor melts

principally derived from the asthenosphere will experience slab tear and first metasomatise and later initiate the melting of previously metasomatised lithosphere.

Mica-bearing lamprophyres (minettes) are restricted to late Miocene time in a post collisional tectonic setting in which melts originated from enriched sub-continental lithospheric mantle. This emphasises the role of the Neo-Tethyian oceanic crust + sediments subduction and metasomatism as the cause of the enrichment of their source. The intermediate lamprophyres represent batches of magma from lithospheric mantle source that was affected by both types of metasomatism: deep astenospheric mantle melts and subduction-related crustal melts. Intermediate type lamprophyric magmas show that some parts of the mantle are multiply metasomatised, similar to other cases worldwide (e.g., Tappe et al., 2008; Prelević et al., 2012; Abdelfadil et al., 2013).

8. Concluding remarks

Lamprophyric magmatism in the northwestern Iran has been active during long period from Late Cretaceous to Late Oligocene-Early Miocene and Late Miocene times. According to mineralogy, geochemistry and isotopic ratios, the studied lamprophyres can be divided in three major groups: sannaite to camptonite (amphibole-bearing), minette (mica-bearing), and spessartite.

Sannaite and camptonite lamprophyres are restricted to the oldest magmatic events in Late Cretaceous and Late Oligocene-Early Miocene periods. According to their geochemistry and isotopic ratios they originated from a lithospheric mantle affected by the melts ultimately derived from the convecting mantle.

Minettes have a late Miocene age and their geochemistry and isotopic ratios indicate a clear subduction-related signature in a collision type geodynamic environment. Minette type lamprophyres originated from metasomatised lithospheric mantle affected by subduction related agents.

Spessartite type lamprophyres are coeval with minette showing geochemical features transitional between minette and sannaite/camptonite lamprophyres originated from a lithospheric mantle metasomatised by subduction related and deep asthenospheric mantle agents.

Acknowledgments

Funding for major and trace element analyses was provided by Payame Noor University. Mr. Maurizio Ulivi and Prof. Riccardo Avanzinelli are acknowledged for help during isotopic analyses, which have been performed with the financial support of PRIN 2010-2011 funds (grant # 2010TT22SC_001). Grateful thanks are extended to Sebastian Fischer for help during microprobe analyses of Iranian samples. D.P. was supported through the Geocycles Research Centre of the University of Mainz. The final version of the paper has benefited from the perceptive comments of Stephen Foley. We truly appreciate the insightful reviews provided by Sebastian Tappe and K.N. Pang, and the editorial help and patience of Nelson Eby.

References

Abdelfadil, K.M., Romer, R.L., Seifert, T., Lobst, R., 2013. Calc-alkaline lamprophyres from Lusatia (Germany) Evidence for a repeatedly enriched mantle source. Chemical Geology 353, 230–245.

Adamia, S., Zakariadze, G., Chkhotua, T., Sadradze, N., Tsereteli, N., Chabukiani, A., Gventsadze, A., 2011. Geology of the Caucasus: a review. Turkish Journal of Earth Science 20, 489-544.

Aghazadeh, M., 2009. Petrology and Geochemistry of Anzan, Khankandi and Shaivar Dagh granitoids (North and East of Ahar, Eastern Azerbaijan) with references to associated mineralization. Unpublished PhD thesis, Tarbiat Modares University, Iran, 470 pp.

Aghazadeh, M., Badrzadeh, Z., 2012. Mineralogy and petrogenesis of alkaline and calc-alkaline lamprophyres in the northwestern Iran: implication for mantle heterogeneity. International earth science colloquium on the Aegean region, IESCA, Izmir, Turkey.

Aghazadeh, M., Castro, A., Badrzadeh, Z., Vogt, K., 2011. Post-collisional polycyclic plutonism from the Zagros hinterland. The Shaivar-Dagh plutonic complex Alborz belt, Iran. Geological Magazine 148, 980-1008.

Aghazadeh, M., Castro, A., Rashidnejad Omran, N., Emami, M.H., Moinvaziri, H., Badrzadeh, Z., 2010. The gabbro (shoshonitic)–monzonite–granodiorite association of Khankandi pluton, Alborz Mountains, NW Iran. Journal of Asian Earth Sciences 38, 199-219.

Allan, J.F., Carmichael, I.S.E., 1984. Lamprophyric lavas in the Colima graben, SW Mexico. Contributions to Mineralogy and Petrology 88, 203-216.

Allen, M.B., Armstrong, H.A., 2008. Arabia–Eurasia collision and the forcing of mid-Cenozoic global cooling. Palaeogeography Palaeoclimatology Palaeoecology 265, 52-58.

Avanzinelli, R., Boari, E., Conticelli, S., Francalanci, L., Guarnieri, L., Perini, G., Petrone, C.M., Tommasini, S., Ulivi, M., 2005. High precision Sr, Nd, and Pb isotopic analyses and reproducibility using new generation thermal ionisation mass spectrometer: aims and perspective for isotope geology applications. Periodico di Mineralogia 75, 187-207.

Avanzinelli, R., Braschi, E., Marchionni, S., Bindi, L., 2014. Mantle melting in within-plate continental settings: Sr–Nd–Pb and U-series isotope constraints in alkali basalts from the Sicily Channel (Pantelleria and Linosa Islands, Southern Italy). Lithos 188, 213-228

Avanzinelli, R., Elliott, T., Tommasini, S., Conticelli, S., 2008. Constraints on the genesis of the potassium-rich Italian volcanics from U/Th disequilibrium. Journal of Petrology 49, 195-223.

Avanzinelli, R., Prytulak, J., Skora, S., Heumann, A., Koetsier, G., Elliott, T., 2012b. Combined ^{238}U-^{230}Th and ^{235}U-^{231}Pa constraints on the transport of slab-derived material beneath the Mariana Islands. Geochimica et Cosmochimica Acta 92, 308-328.

Avanzinelli, R., Sapienza, G., Conticelli, S., 2012a. The Cretaceous to Paleogene within-plate magmatism of Pachino-Capo Passero (southeastern Sicily) and Adria (La Queglia and Pietre Nere, southern Italy): geochemical and isotopic evidence against a plume-related origin of circum-Mediterranean magmas. European Journal of Mineralogy 24, 73-96.

Azizi, H., Jahangiri, A., 2008. Cretaceous subduction-related volcanism in the northern Sanandaj-Sirjan Zone, Iran. Journal of Geodynamics 45, 178-190.

Azizi, H., Zanjefili Beiranvand, M., Asahara, Y., 2014. Zircon U–Pb ages and petrogenesis of a tonalite–trondhjemite–granodiorite (TTG) complex in the northern Sanandaj–Sirjan Zone, northwest Iran: evidence for Late Jurassic arc-continent collision. Lithos in press, doi: 10.1016/j.lithos.2014.11.012.

Babakhani, A.R., Lesquyer, J.L., Rico, R., 1990. Geological Map of Ahar Quadrangle (scale 1:250,000). Geological Survey of Iran, Tehran, Iran.

Bazhenov, M., Burtman, V.S., Levashova, N.M., 1996. Lower and Middle Jurassic paleomagnetic results from the south Lesser Caucasus and the evolution of the Mesozoic Tethys ocean. Earth and Planetary Science Letters 141, 79-89.

Beccaluva, L., Bianchini, G., Bonadiman, C., Siena, F., Vaccaro, C., 2004. Coexisting anorogenic and subduction related metasomatism in mantle xenoliths from the Betic Cordillera (Southern Spain). Lithos 75, 67-87.

Berberian, M., King, G.C.P., 1981. Towards a paleogeography and tectonic evolution of Iran. Canadian Journal of Earth Sciences 18, 210-265.

Bianchini, G., Beccaluva, L., Nowell, G.M., Pearson, D.G, Siena, F., 2010. Mantle xenoliths from Tallante (Betic Cordillera): Insights into the multi-stage evolution of the south Iberian lithosphere. Lithos 124, 308-318.

Boari, E., Avanzinelli, R., Melluso, L., Giordano, G., Mattei, M., Morra, V., Conticelli, S., 2009a. Isotope geochemistry (Sr-Nd-Pb) and petrogenesis of leucite-bearing volcanic rocks from “Colli Albani” volcano, Roman Magmatic Province, Central Italy: inferences on volcano evolution and magma genesis. Bulltin of Volcanology 71, 977-1005.

Boari, E., Tommasini, S., Laurenzi, M.A., Conticelli, S., 2009b. Transition from ultrapotassic kamafugitic to sub-alkaline magmas: Sr, Nd, and Pb isotope, trace element and ^{40}Ar-^{39}Ar age data from the Middle Latin Valley volcanic field, Roman Magmatic Province, Central Italy. Journal of Petrology 50, 1327-1357.

Carmichael, I.S.E., Lange, R.A., Luhr, J.F., 1996. Quaternary minettes and associated volcanic rocks of Mascota, western Mexico: a consequence of plate extension above a subduction modified mantle wedge. Contribution to Mineralogy Petrology, 124, 302-333.

Cellai, S., Conticelli, S., Menchetti, S., 1994. Crystal-chemistry of clinopyroxenes from potassic and ultrapotassic rocks in Central Italy: implications on their genesis. Contributions to Mineralogy and Petrology, 116, 301-315.

Class, C., Goldstein, S.L., 1997. Plume lithosphere interaction in the ocean basins: constraints from the source mineralogy. Earth Planetary Science Letters 150, 245-260.

Conceição, R.V., Green, D.H., 2004. Derivation of potassic (shoshonitic) magmas by decompression melting of phlogopite+pargasite lherzolite. Lithos 72, 209-229.

Conticelli, S., 1998. Effects of Crustal Contamination on Ultrapotassic Magmas with Lamproitic Affinity: Mineralogical, Geochemical and Isotope data from the Torre Alfina Lavas and Xenoliths, Central Italy. Chemical Geology 149, 51-81.

Conticelli, S., Avanzinelli, R., Marchionni, S., Tommasini, S., Melluso, L., 2011. Sr-Nd-Pb isotopes from the Radicofani Volcano, Central Italy: constraints on heterogeneities in a veined mantle responsible for the shift from ultrapotassic shoshonite to basaltic andesite magmas in a post-collisional setting. Mineralogy and Petrolology 103, 123-148.

Conticelli, S., Avanzinelli, R., Poli, G., Braschi, E., Giordano, G., 2013. Shift from lamproite-like to leucititic rocks: Sr-Nd-Pb isotope data from the Monte Cimino volcanic complex vs. the Vico stratovolcano, Central Italy. Chemical Geology 353, 246-266.

Conticelli, S., Carlson, R.W., Widom, E., Serri, G., 2007. Chemical and isotopic composition (Os, Pb, Nd, and Sr) of Neogene to Quaternary calc-alkalic, shoshonitic, and ultrapotassic mafic rocks from the Italian peninsula: Inferences on the nature of their mantle sources. In: Beccaluva, L., Bianchini, G., Wilson. M., (Eds.), Cenozoic Volcanism in the Mediterranean Area. Geological Society America Special Paper, pp. 171-202.

Conticelli, S., D'Antonio, M., Pinarelli, L., Civetta, L., 2002. Source contamination and mantle heterogeneity in the genesis of Italian potassic and ultrapotassic volcanic Rocks: Sr-Nd-Pb Isotope data from Roman Province and Southern Tuscany. Mineralogy and Petrology 74, 189-222.

Conticelli, S., Guarnieri, L., Farinelli, A., Mattei, M., Avanzinelli, R., Bianchini, G., Boari, E., Tommasini, S., Tiepolo, M., Prelévic, D., Venturelli, G., 2009a. Trace elements and Sr-Nd-Pb isotopes of K-rich to shoshonitic and calc-alkalic magmatism of the Western Mediterranean region: genesis of ultrapotassic to calc-alkalic magmatic associations in post-collisional geodynamic setting. Lithos 107, 68-92.

Conticelli, S., Manetti, P., Menichetti, S., 1992. Petrology, Chemistry, Mineralogy and Sr-isotopic features of Pliocenic Orendites from South Tuscany: implications on their genesis and evolutions. European Journal of Mineralogy 4, 1359-1375.

Conticelli, S., Marchionni, S., Rosa, D., Giordano, G., Boari, E., Avanzinelli, R., 2009b. Shoshonite and sub-alkaline magmas from an Ultrapotassic Volcano: Sr-Nd-Pb isotope data on the Roccamonfina volcanic rocks, Roman Magmatic Province, Southern Italy. Contribution to Mineralogy and Petrology 157, 41-63.

Conticelli, S., Melluso, L., Perini, G., Avanzinelli, R., Boari, E., 2004. Petrologic, geochemical, and isotopic characteristics of potassic and ultrapotassic magmatism in central-southern Italy: inferences on its genesis and on the nature of mantle sources. Periodico Mineralogy 73, 153-164.

Conticelli, S., Peccerillo A., 1992. Petrology and geochemistry of potassic and ultrapotassic volcanism in central Italy: petrogenesis and inferences on the evolution of the mantle sources. Lithos 28, 221-240.

Dalrymple, G.B., Duffield, W.A., 1988. High Precision $^{40}Ar/^{39}Ar$ Dating of Oligocene Rhyolites from the Mogollon-Datil Volcanic Field Using a Continuous Laser System. Geophysical Research Letters 15, 463–466.

Davies, J.H., Von Blanckenburg, F., 1995. Slab breakoff: a model of lithosphere detachment and its test in the magmatism and deformation of collisional orogens. Earth and Planetary Science Letters 129, 85-102.

DePaolo, D.J., 1981. Trace element and isotopic effects of combined wall rock assimilation and fractional crystallization. Earth and Planetary Science Letters 53, 189-202.

Dewey, J.F., 1988. Extensional collapse of orogens. Tectonics 7, 1123-1139.

Dilek, Y., Imamverdiyev, N., Altunkaynak, S., 2009. Geochemistry and tectonics of Cenozoic volcanismin the Lesser Caucasus (Azerbaijan) and the peri-Arabian region: Collision induced mantle dynamics and its magmatic fingerprint. International Geology Review 52, 536–578.

Doe, B.R., Zartman, R.E., 1979. Plumbotectonics I, the Phanerozoic, In: Barnes, H.L., (Ed.), Geochemistry of Hydrothermal Ore Deposits, 2nd edition. John Wiley and Sons, New York, pp. 22-70.

Dostal, J., Owen, J.V., 1998. Cretaceous alkaline lamprophyres from north-eastern Czech Republic: geochemistry and petrogenesis. Geologische Rundschau 87, 67–77.

Edwards, C.M.H., Menzies, M.A., Thirlwall, M.F., Morris, J.D., Leeman, W.P., Harmon, R.S., 1994. The transition to potassic alkaline volcanism in Island arcs: The Ringgit-Beser complex, East Java, Indonesia. Journal of Petrology 35, 1557-1595.

Elliott, T., Plank, T., Zindler, A., White, W., Bourdon, B., 1997. Element transport from slab to volcanic front at the Mariana arc. Journal of Geophysical Research 102, 14991-15019

Falloon, T.J., Green, D.T., Hatton, C.J., Harris, K.L., 1988. Anhydrous partial melting of a fertile and depleted peridotite from 2 to 30 kbar and application to basalt petrogenesis. Journal of Petrology 29, 1257-1282.

Foley, S.F., 1992a. Petrological characterization of the source components of potassic magmas: geochemical and experimental constraints. Lithos 28, 187-204

Foley, S.F., 1992b. Vein-plus-wall-rock melting mechanisms in the lithosphere and the origin of potassic alkaline magmas. Lithos 28, 435-453

Foley, S.F., Jackson, S.E., Fryer, J.D., Greenough, G.A.J., 1996. Trace element partition coefficients for clinopyroxene and phlogopite in an alkaline lamprophyre from Newfoundland by LAM-ICP-MS. Geochimica et Cosmochimca Acta 60, 629–638.

Foley, S.F., Venturelli, G., Green, D.H., Toscani, L., 1987. The ultrapotassic rocks: characteristics, classification and constraints for petrogenetic models. Earth-Science Reviews 24, 81-134.

Foley, S.F., Musselwhite, D.S., Van der Laan, S.R., 1999. Melt compositions from ultramafic vein assemblages in the lithospheric mantle: a comparison of cratonic and non-cratonic settings. Proceedings of the 7th International KimberliteConference, pp. 238‑246 (J.B. Dawson Volume).

Frey, F.A., Green, D.H., Roy, S.D., 1978. Integrated Models of Basalt Petrogenesis: A Study of Quartz Tholeiites to Olivine Melilitites from South Eastern Australia Utilizing Geochemical and Experimental Petrological Data. Journal of Petrology 19, 463-513.

Fritschle, T., Prelević, D., Foley, S.F., Jacob, D.E., 2013. Petrological characterization of the mantle source of Mediterranean lamproites: Indications from major and trace elements of phlogopite. Chemical Geology 30, 267-279.

Furman, T., Graham, D., 1999. Erosion of lithospheric mantle beneath the east African rift system; geochemical evidence from the Kivu volcanic province. Lithos 48, 237–262.

Ghalamghash, J., Nédélec, A., Bellon, H., Vousoughi Abedini, M., Bouchez, J.L., 2009. The Urumieh plutonic complex (NW Iran): A record of the geodynamic evolution of the Sanandaj–Sirjan zone during Cretaceous times - Part I: Petrogenesis and K/Ar dating. Journal of Asian Earth Sciences 35, 401-415.

Gibson, S.A., Thompson, R.N., Leonardos, O.H., Dickin, A.P, Mitchell, J.G., 1995. The Late Cretaceous impact of the Trindade mantle plume: evidence from large-volume, mafic, potassic magmatism in SE Brazil. Journal of Petrology 36, 189-229.

Hart, S.R., 1984. A large isotope anomaly in the southern hemisphere mantle. Nature 309, 753-757.

Hofmann, A.W., 1997. Mantle geochemistry: the message from oceanic volcanism. Nature 385, 219–229.

Hofmann, A.W., White, W.M., 1982. Mantle plumes from ancient oceanic crust. Earth and Planetary Science Letters 57, 421–436.

Jahn, B.M., Wu, F.Y., Lo, C.H., Tsai, C.H., 1999. Crust-mantle interaction induced by deep subduction of the continental crust: geochemical and Sr-Nd isotopic evidence from post-collisional mafic-ultramafic intrusions of the northern Dabie complex,central China. Chemical Geology 157, 119-146.

Khalatbari-Jafari, M., Juteau, T., Cotten, J., 2006. Petrological and geochemical study of the Late Cretaceous ophiolite of Khoy (northwestern Iran), and related geological formations. Journal of Asian Earth Sciences 27, 465–502.

Kuno, H., 1968. Differentiation of basalt magmas. In: Hess, H.H., Poldervaart, A., (Eds.), Basalts: The Poldervaart Treatise on Rocks of Basaltic Composition. Wiley Interscience, New York, pp. 623-688.

Lange, R.A., Carmichael I.S.E., 1990. Hydrous basaltic andesites associated with minette and related lavas in western Mexico. Journal of petrology 31, 1225-1259.

Le Maitre, R.W., 2002. Igneous Rocks: A Classification and Glossary of Terms: Recommendations of the International Union of Geological Sciences Subcommission on the Systematics of Igneous Rocks. Cambridge University Press, Cambridge. 236 pp.

Lee, M.J., Lee, J.I., Choe, W.H., Park, C.H., 2008. Trace element and isotopic evidence for temporal changes of the mantle sources in the South Shetland Islands, Antarctica. Geochemical Journal 42, 207 – 219.

Lustrino, M., Wilson, M., 2007. The circum-Mediterranean anorogenic Cenozoic Igneous Provinces. Earth Science Review 81, 1-55.

Mederer, J., Moritz, R., Ulianov, A., Chiaradia, M., 2013. Middle Jurassic to Cenozoic evolution of arc magmatism during Neotethys subduction and arc-continent collision inthe Kapan Zone, southern Armenia. Lithos 177, 61–78.

Mirnejad, H., Bell, K., 2006. Origin and source evolution of the Leucite Hills lamproites: evidence from Sr–Nd–Pb– O isotopic compositions. Journal of Petrology 47, 2463-2489.

Mitchell, R.H., Bergman, S.C., 1991. Petrology of Lamproites. Plenum Press, New York. 447 pp.

Moayyed, M., Moazzen, M., Calagari, A.A., Jahangiri, A., Modjarrad M., 2008. Geochemistry and petrogenesis of lamprophyric dykes and the associated rocks from Eslamy peninsula, northwestern Iran: Implications for deep-mantle metasomatism. Chemie der Erde Geochemistry 68, 141-154.

Moinvaziri, H., 1985. Volcanisme tertiaire et quaternaire en Iran. Université Paris-Sud, Orsay, These d'Etat. 278 pp.

Moradian-Shahrbabaky, A., 1997. Geochemistry, Geochronology, and Petrology of Feldspathoid-bearing Rocks in the Urumieh-Dokhtar Volcanic belt, Iran. PhD Thesis, University of Wollongonge, Australia, 411 pp.

Muller, D., Rock, N.M.S., Groves, D.I., 1992. Geochemical discrimination between shoshonitic and potassic volcanic rocks from different tectonic settings, a pilot study. Mineralogy and Petrology 46, 259–289.

Murphy, D.T., Collerson, K.D., Kamber, B.S., 2002. Lamproites from Gaussberg, Antarctica, possible transition zone melts of Archean subducted sediments. Journal of Petrology 43, 981-1001.

Owen, J.P., 2008. Geochemistry of lamprophyres from the Western Alps, Italy: implications for the origin of an enriched isotopic component in the Italian mantle. Contribution to Mineralogy and Petrology 155, 341–362.

Pang, K.N., Chung, S.L., Zarrinkoub, H.S., Lin, Y.C., Lee, H.Y., Lo, C.H., Khatib, M.M., 2013. Iranian ultrapotassic volcanism at ~11 Ma signifies the initiation of postcollisional magmatism in the Arabia-Eurasia collision zone. Terra Nova 25, 405–413.

Peccerillo, A., Martinotti, G., 2006. The Western Mediterranean lamproitic magmatism: origin and geodynamic significance. Terra Nova 18, 109-117.

Perini, G., Francalanci, L., Davidson, J.P., Conticelli, S., 2004. Evolution and genesis of magmas from Vico Volcano, Central Italy: multiple differentiation pathways and variable parental magmas. Journal of Petrology 45, 139-182.

Pilet, S., Hernandez, J., Sylvester, P., 2005. The metasomatic alternative for ocean island basalt chemical heterogeneity. Earth and Planetary Science Letters 236, 148-166.

Pilet, S., Baker, M.B., Stolper, E.M., 2008. Metasomatized lithosphere and the origin of alkaline lavas. Science 320, 916-919.

Plank, T., 2005. Constraints from thorium/lanthanum on sediment recycling at subduction zones and the evolution of the continents. Journal of Petrology 46, 921-944.

Plank, T., Langmuir, C.H., 1998. The chemical composition of subducting sediment and its consequences for the crust and mantle. Chemical Geology 145, 325–394.

Prelević, D., Akal, C., Foley, S.F., Romer, R.L., Stracke, A., Van Den Bogaard, P., 2012. Ultrapotassic mafic rocks as geochemical proxies for postcollisional mantle dynamics of lithosphere: the case of SW Anatolia-Turkey. Journal of Petrology 53, 1019-1055.

Prelević, D., Foley, S.F., Cvektović, V., Romer, R.L., 2004. Origin of Minette by Mixing of Lamproite and Dacite Magmas in Veliki Majdan, Serbia. Journal of petrology, 45, 759-792.

Prelević, D., Foley, S.F., Romer, R.L., Conticelli, S., 2008. Mediterranean Tertiary lamproites derived from multiple source components in postcollisional geodynamics. Geochimica et Cosmochimica Acta 72, 2125-2156.

Prelević, D., Foley, S.F., Romer, R.L., Cvetković, V., Downes, H., 2005. Tertiary Ultrapotassic Volcanism in Serbia: Constraints on Petrogenesis and Mantle Source Characteristics. Journal of Petrology 46, 1443-1487.

Prelević, D., Seghedi, I., 2013. Magmatic response to the post-accretionary orogenesis within Alpine-Himalayan belt. Lithos 180, 1-4.

Prelević, D., Stracke, A., Foley, S.F., Romer, R.L., Conticelli, S., 2010. Hf isotope compositions of Mediterranean lamproites: Mixing of melts from asthenosphere and crustally contaminated mantle lithosphere. Lithos 119, 297-312.

Rock, N.M.S., 1977. The Nature and Origin of Lamprophyres: Some definitions, classifications and derivations. Earth Science Review 13, 123-169.

Rock, N.M.S., 1991. Lamprophyres. Blackie and Son, Glasgow, 285pp.

Rolland, Y., Galoyan, G., Bosch, D., Sosson, M., Corsini, M., Fornari, M., Verati, C., 2009. Jurassic back-arc and Cretaceous hot-spot series In the Armenian ophiolites - implications for the obduction process. Lithos 112, 163–187.

Rudnick, R.L., Gao, S., 2003. Composition of the continental crust. In: Holland H.D., Turekian K.K., (Eds.), Treatise on Geochemistry 3, The crust. Elsevier Pergamon Oxford, pp.1-64.

Seghedi, I., Downes, H., Vaselli, O., Szakács, A., Balogh, K., Pécskay, Z., 2004. Post-collisional Tertiary–Quaternary mafic alkalic magmatism in the Carpathian–Pannonian region: a review. Tectonophysics 393, 43-62.

Sosson, M., Rolland, Y., Mller, C., Danelian, T., Melkonyan, R., Kekelia, S., Adamia, S., Babazadeh, V., Kangarli, T., Avagyan, A., Galoyan, G., Mosar, J., 2010. Subductions,

obduction and collision in the Lesser Caucasus (Armenia, Azerbaijan, Georgia), new insights. Geological Society of London, Special Publications 340, 329–352.

Stacey, J.S., Kramers, J.D., 1975. Approximation of terrestrial lead isotope evolution by a two - stage model. Earth and Planetary Science Letters 26, 207-221.

Stampfli, G.M., Borel, G.D., 2002. A plate tectonic model for the Paleozoic and Mesozoic constrained by dynamic plate boundaries and restored synthetic oceanic isochrons. Earth and Planetary Science Letters 196, 17-33.

Staudigel, H., Davies, G.R., Hart, S.R., Marchant, K.M., Smith, B.M., 1995. Large scale isotopic Sr, Nd and O isotopic anatomy of altered oceanic crust: DSDP/ODP sites 417/418. Earth Planetary Science Letters 130, 169-185.

Streckeisen, A., 1978. Classification and nomenclature of volcanic rocks, lamprophyres, carbonatites and melilitic rocks: recommendations and suggestions, IUGS Subcommission on the Systematics of Igneous Rocks. Neues Jahrbuch fur Mineralogie, Abhandlungen 134, 1-14.

Sun, S.S., McDonough, W.F., 1989. Chemical and isotopic systematics of oceanic basalts: implications for mantle composition and processes. Geological Society, London, Special Publications 42, 313-345.

Tappe, S., Foley, S.F., Jenner, G.A., Heaman, L.M., Kjarsgaard, B.A., Romer, R.L., Stracke, A., Joyce, N., Hoefs, J., 2006. Genesis of ultramafic lamprophyres and carbonatites at Aillik Bay, Labrador: A consequence of incipient lithospheric thinning beneath the North Atlantic craton. Journal of Petrology 47, 1261-1315.

Tappe, S., Jenner, G.A., Foley, S.F., Heaman, L.M., Besserer, D., Kjarsgaard, B.A., Ryan, B., 2004. Torngat ultramafic lamprophyres and their relation to the North Atlantic Alkaline Province. Lithos 76, 491–518.

Tappe, S., Foley, S.F., Jenner, G.A., Kjarsgaard, B.A., 2005. Integrating ultramafic lamprophyres into the IUGS classification of igneous rocks: rational and implications. Journal of Petrology 46, 1893-1900.

Tappe, S., Foley, S.F., Kjarsgaard, B.A., Romer, R.L., Heaman, L.M., Stracke, A., Jenner, G.A., 2008. Between carbonatite and lamproite - diamondiferous Torngat ultramafic lamprophyres formed by carbonate-fluxed melting of cratonic MARID-type metasomes. Geochimica et Cosmochimica Acta 72, 3258–3286.

Tappe, S., Foley, S.F., Stracke, A., Romer, R.L., Kjarsgaard, B.A., Heaman, L.M., Joyce, N., 2007. Craton reactivation on the Labrador Sea margins: $^{40}Ar/^{39}Ar$ age and Sr–Nd–Hf–Pb isotope constraints from alkaline and carbonatite intrusives. Earth and Planetary Science Letters 256, 433-454.

Taylor, S.R., McLennan, S.M., 1985. The Continental Crust: Its Composition and Evolution. Blackwell Scientific Publications, Oxford, pp. 1-312.

Thirlwall, M.F., 2000. Inter-laboratory and other errors in Pb isotope analyses investigated using a ^{207}Pb-^{204}Pb double spike. Chemical Geology 163, 299-322.

Thompson, R.N., Leat, P.T., Dickin, A.P., Morrison, M.A., Hendry, G.L., Gibson, S.A., 1990. Strongly potassic mafic magmas from lithospheric mantle sources during continental extension and heating. Earth and Planetary Science Letters 98, 139–153.

Tiepolo, M., Tribuzio, R., Vannucci, R., 2002. The composition of mantle-derived melts developed during the Alpine continental collision. Contributions to Mineralogy and Petrology 144, 1-15.

Tommasini, S., Avanzinelli, R., Conticelli, S., 2011. The Th/La and Sm/La conundrum of the Tethyan realm lamproites. Earth and Planetary Science Letters 301, 469-478.

Turner, S.P., Arnaud, N., Liu, J., Rogers, N., Hawkesworth, C.J., Harris, N., Kelley, S., van Calsteren, P., Deng, W., 1996. Post-collision, shoshonitic volcanism on the Tibetan Plateau: implications for convective thinning of the lithosphere and the source of ocean island basalts. Journal of Petrology 37, 45-61.

Turner, S.P., Platt, J.P., George, R.M.M., Kelley, S.P., Pearson, D.G., Nowell, G.M., 1999. Magmatism associated with orogenic collapse of the Betic-Alboran domain, SE Spain. Journal of Petrology 40, 1011-1036.

Van den Bogaard, P., 1995. $^{40}Ar/^{39}Ar$ ages of sanidine phenocrysts from Laacher See Tephra(12,900 yr BP): Chronostratigraphic and petrological significance. Earth and Planetary Science Letters 133, 163-174.

Wagner, C., Velde, D., 1986. The mineralogy of K-richterite bearing lamproite. Americam Mineralogist 71, 17-37.

Wallace, P., Carmichael, I.S.E., 1989. Minette lavas and associated leucitites from the Western Front of the Mexican Volcanic Belt: petrology, chemistry, and origin. Contributions to Mineralogy and Petrology 103, 470–492.

Wallace, P., Carmichael, I.S.E., Righte,r K., Becker, T.A., 1992. Volcanism and tectonism in western Mexico: a contrast of style and substance. Geology 20, 625-628.

Wilson, M., 1989. Igneous Petrogenesis: A Global Tectonic Approach. Chapman and Hall, London, 466 pp.

Wimmenauer, W., 1973. Lamprophyre, Semilamprophyre und anchibasaltische Ganggesteine. Fortschr Mineralogy 51, 3-67.

Zhang, H., Thurber, C.H., Shelly, D., Ide, S., Beroza, G.C., Hasegawa, A., 2003. High-resolution Subducting slab structure beneath northern Honshu, Japan, revealed by Double-Difference tomography. Geology 32, 361-364.

Zindler, A., Hart, S., 1986. Chemical geodynamics. Annual Review of Earth and Planetary Sciences 14, 493–571.

Captions

Fig. 1: (a) Geological map of Iran with different structural units and position of Paleo and Neotethys suture lines; (b) Geological map of northwestern Iran and location of studied lamprophyres.

Fig. 2: Microphotographs of studied lamprophyres; (a) brown amphibole phenocrysts with kaersutitic composition in the Khankandi camptonites; (b) Olivine pseudomorph in Sorkheh spessrtite; (c) porphyritic texture with amphibole and clinopyroxene phenocrysts in feldspar and chlorite matrix; (d) Phlogopite phenocryst with compositional zoning in Eslamy minette. Pictures a, c and d take under plane-polarized light and b take under crossed polars.

Fig. 3: (a) Total alkali vs. silica diagram (Le Maitre, 2002) shows all studied lamprophyres located above Kuno (1968) alkali line and in the alkaline field. (b) CaO vs. Al_2O_3 diagram show the Eslamy minettes mainly located in the Roman province field. Base diagram after Foley et al. (1987).

Fig. 4: Major elements variation diagrams for different minerals of studied lamprophyres. (a) Al vs. Ti expressed as atoms per formula unit (a.f.u.) for clinopyroxene from studied lamprophyres. Fields for clinopyroxe in lamproites and Roman-type rocks after Conticelli (1998), fields of clinopyroxene from Italian lamproites after Conticelli et al. (1992), Cellai et al. (1994), Conticelli (1998). Note camptonite clinopyroxene show higher TiO_2 and Al_2O_3 and spessartite clinopyroxene plot between sannaite/camptonite and minette fields. (b) #Mg vs. SiO_2 diagram shows studied minette micas have lower SiO_2 than Mediterranean lamproites and Eslamy minettes mica shift toward Mediterranean lamproite field. Eslamy minette micas represent higher SiO_2 and #Mg than Marand minette micas. Mediterranean lamproite mica data after Wagner and Velde (1986); Conticelli et al. (1992); Conticelli (1998); Prelević et al. (2008). (c) Al_2O_3 vs. TiO_2 diagram show studied minette micas located in the field of minette and Roman province micas. Different rocks mica fields after Mitchell and Bergman (1991). (d) Amphiboles composition from Horand sannaite and Khankandi camptonite in the TiO_2 vs. SiO_2 diagram. Studied amphiboles located in the field proposed for alkaline lamprophyres. Diagram and fields of amphiboles in the different lamprophyres after Rock (1991), fields of Aillik Bay area lamproites and nephelinite after Tappe et al. (2007) and field of Torngat ultramafic lamprophyres after Tappe et al. (2004).

Fig. 5: $^{40}Ar/^{39}Ar$ age spectra for mica (a,b) and amphibole (c,d,e,f) from Marand (a) and Eslamy (b) minettes, Sorkheh spessartite (c,d) and Horand sannaite (e,f).

Fig. 6: Primitive mantle normalised spider diagrams of studied minette (a), sannaite/camptonite (b), and spessartite (c) lamprophyres. Average of minette, camptonite, calc-alkaline, and alkaline lamprophyres after Rock (1991) are added to a and b. (d) Average of OIB, MORB, GLOSS and Mediterranean marlstone and shale-sandstone data to comparison with studied lamprophyres. MORB, OIB and values for normalization in this and primitive mantle normalized value after Sun and McDonough (1989), average of calc-alkaline, and alkaline lamprophyres after Rock (1991), GlOSS-global subducting sediment composition of Plank and Langmuir (1988).

Mediterranean sedimentary data after Conticelli et al. (2009b). See text for discussion.

Fig. 7: Initial Nd–Sr isotopic ratios for studied lamprophyres. Data sources: Arasbaran monzonitic plutons (Aghazadeh et al., 2011), Eslamy peninsula ultrapotassic rocks (Pang et al., 2013), Turkey lamproites (Prelević et al., 2008, Fritschle et al., 2012), Leucite Hills (Mirnejad and Bell, 2006), Circum Mediterranean Anorogenic Cenozoic Igneous (CMACi) rocks (Lustrino and Wilson 2007), Mantle end-members (Zindler and Hart, 1986), Upper Continental Crust (UCC) (Jahan et al., 1999), Subduction sediments (Lee et al., 2008) and central Mediterranean volcanic rocks isotopic data and fields after Conticelli et al. (2002, 2007, 2009a, 2009b 2011, 2013), Perini et al. (2004), Avanzinelli et al. (2008), Prelević et al. (2008, 2010), Boari et al. (2009a, 2009b).

Fig. 8: Variation of $^{207}Pb/^{204}Pb$ vs. $^{206}Pb/^{204}Pb$ (a) and $^{208}Pb/^{204}Pb$ vs. $^{206}Pb/^{204}Pb$ (b) for studied lamprophyres. Mantle, orogen, and upper crust evolution curves are from Doe and Zartman (1979) and the average crustal growth curve (SK line) is from Stacey and Kramers (1975), Circum Mediterranean Anorogenic Cenozoic Igneous (CMACi) rocks (Lustrino and Wilson, 2007), central Mediterranean volcanic rocks isotopic data and fields after Conticelli et al. (2002, 2007, 2009a, 2009b 2011, 2013), Perini et al. (2004), Prelević et al. (2008, 2010), Boari et al. (2009a, 2009b) and NHRL (Northern Hemisphere reference line) after Hart, (1984).

Fig. 9: Evaluation of alteration effect on the chemistry of studied lamprophyres. (a) $^{87}Sr/^{86}Sr$ vs. LOI diagram Horand sannaite and Sorkheh spessartite affected by alteration. This criteria can be confirm by K_2O and Rb vs. LOI diagrams (b and c).

Fig. 10: Variation of initial $^{87}Sr/^{86}Sr$ vs. MgO of the studied lamprophyres that lamprophyres show different arrays. See text for details.

Fig. 11: Sm/La vs.Th/La diagram show minette located in the arc magma array and sannaite/camptonites in the lower part of the Th/La ratio. Sorkheh and Tasuj spessartite located between sannaite/camptonite and minette end members. See text for details. Upper Crust (UC, Rudnick and Gao, 2003), Global subducting Sediment (GlOSS, Plank and Langmuir, 1998), Arc magma array (Plank, 2005) and SaLaTHO and related array (Tommasini et al., 2011).

Fig. 12: Th/Nb vs $^{87}Sr/^{86}Sr$ diagram that show sannaite/camptonite type lamprophyres located in the OIB field while minette type shift toward upper crust. Data for: lamproites from Leucite Hills from Mirnejad and Bell (2006); Mediterranean lamproites from Conticelli et al. (1992, 2002, 2007, 2009a); Owen (2008); Prelević et al. (2010); for upper crust from Rudnick and Gao (2003), the data for OIB are taken from the GEOROC database (http://www.georoc.mpch-mainz.gwdg.de/georoc).

Fig. 13: Th/Yb vs Nb/Yb diagram, sannaite and camptonite fall in mantle array at its OIB end while minette type plots in the arc field. Sorkheh and Tasuj spessartite plot between sannaite/camptonite and minette fields. Diagram and mantle end members after Pearce and Peate (1995).

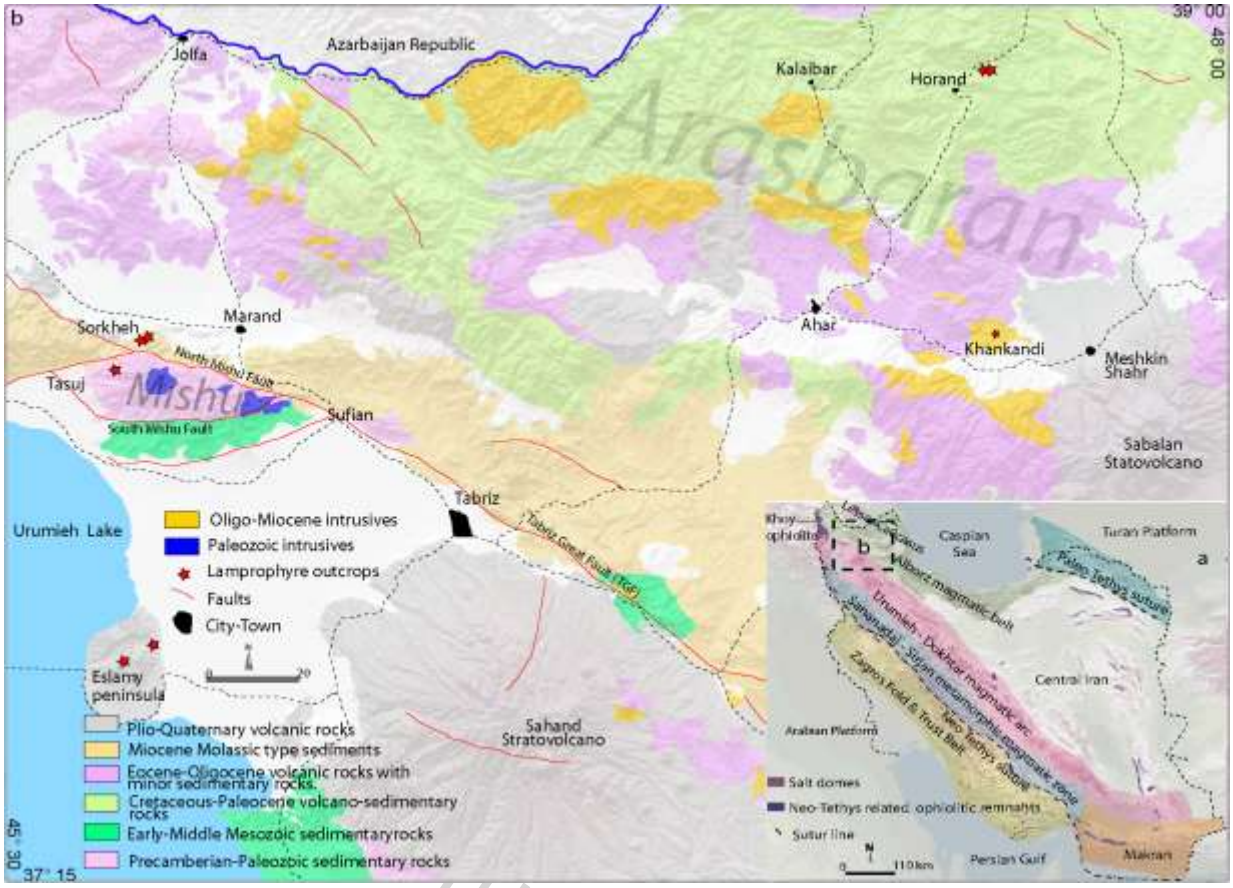

Figure 1

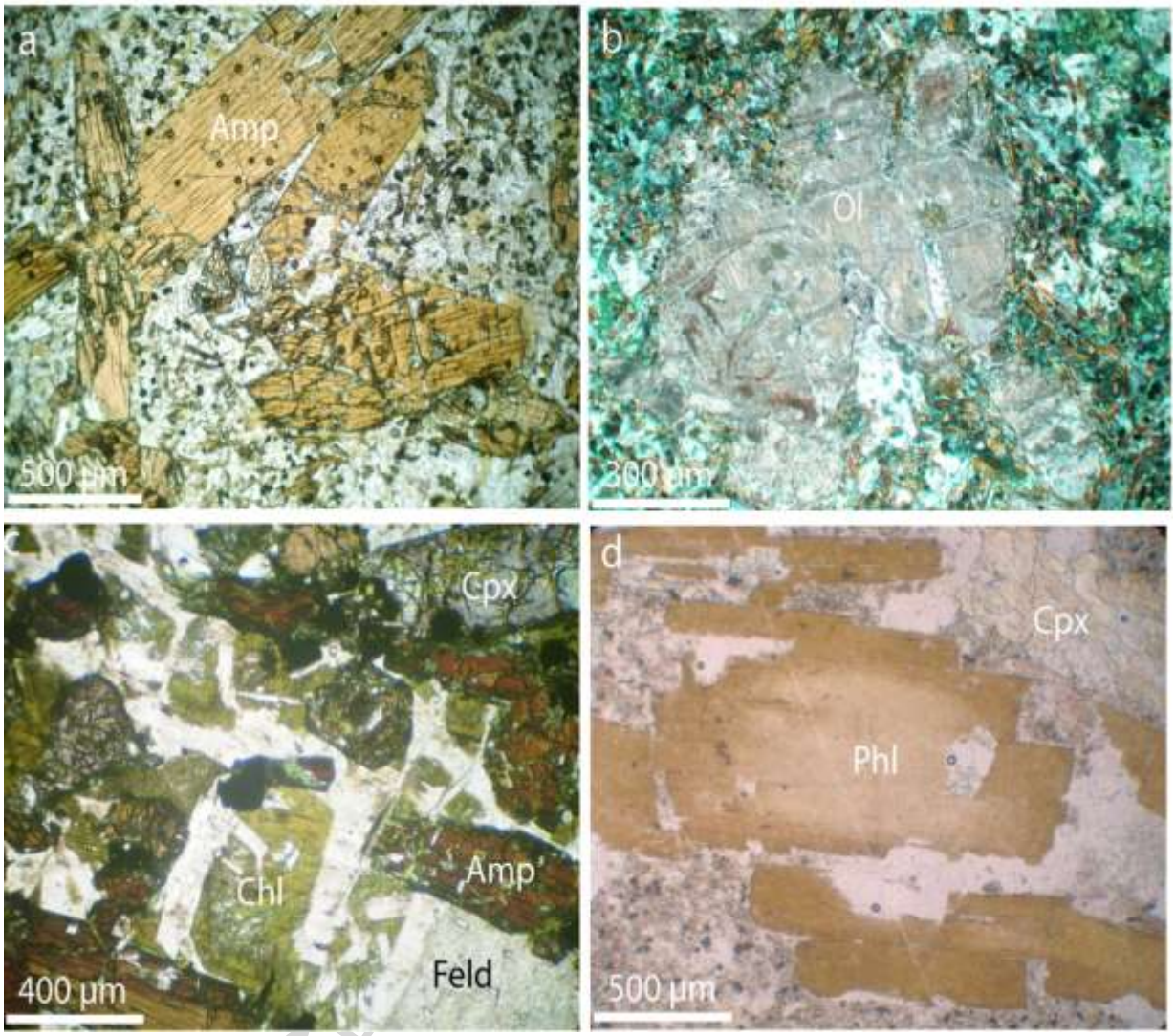

Figure 2

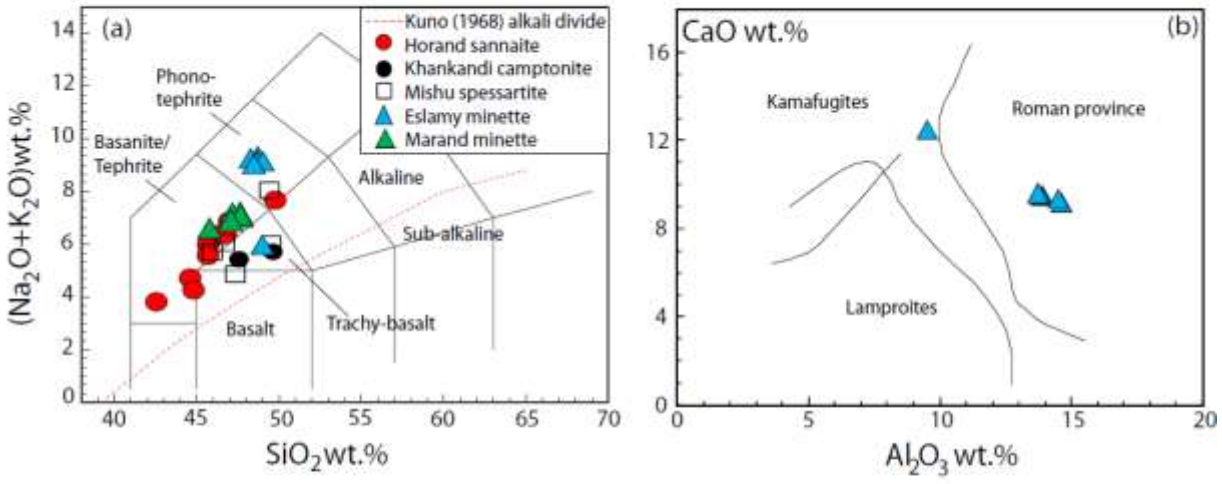

Figure 3

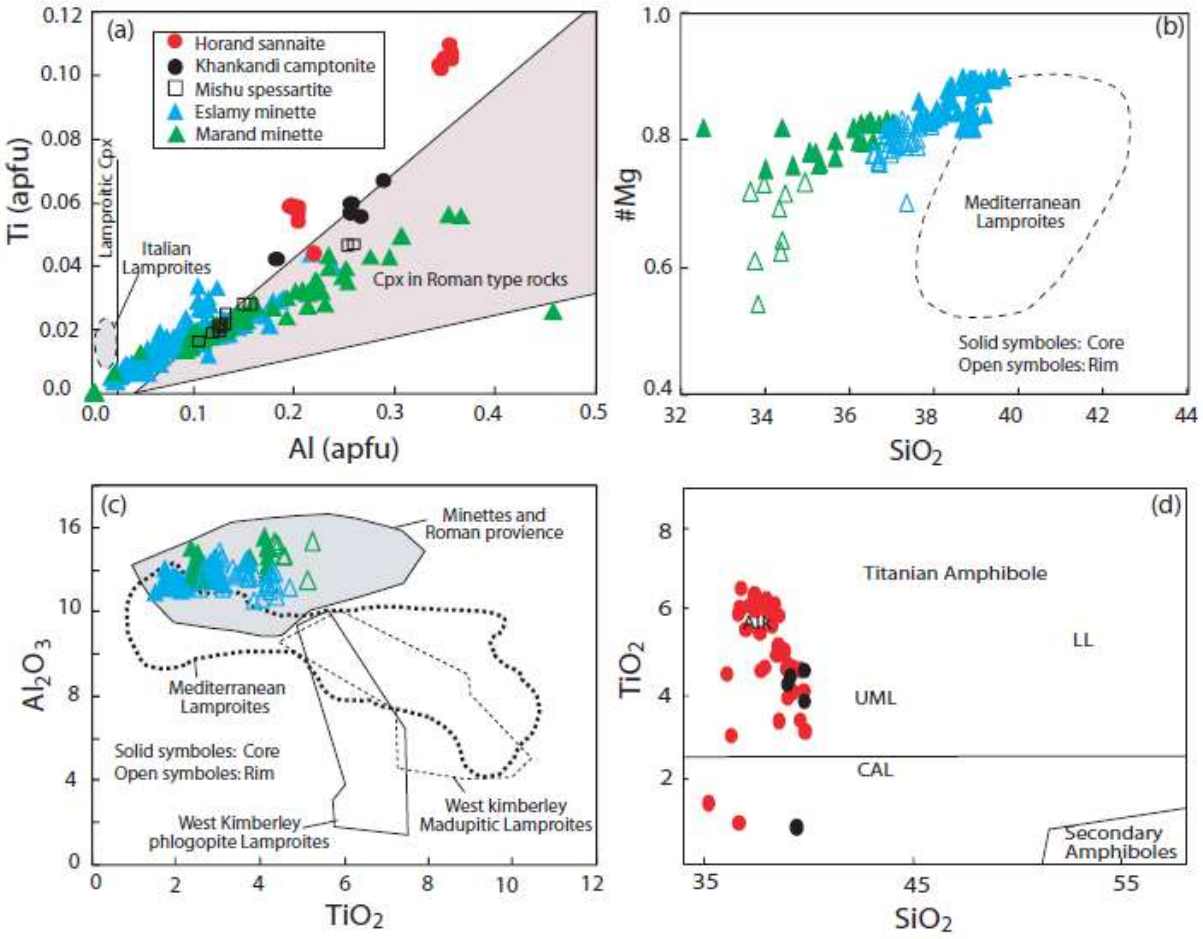

Figure 4

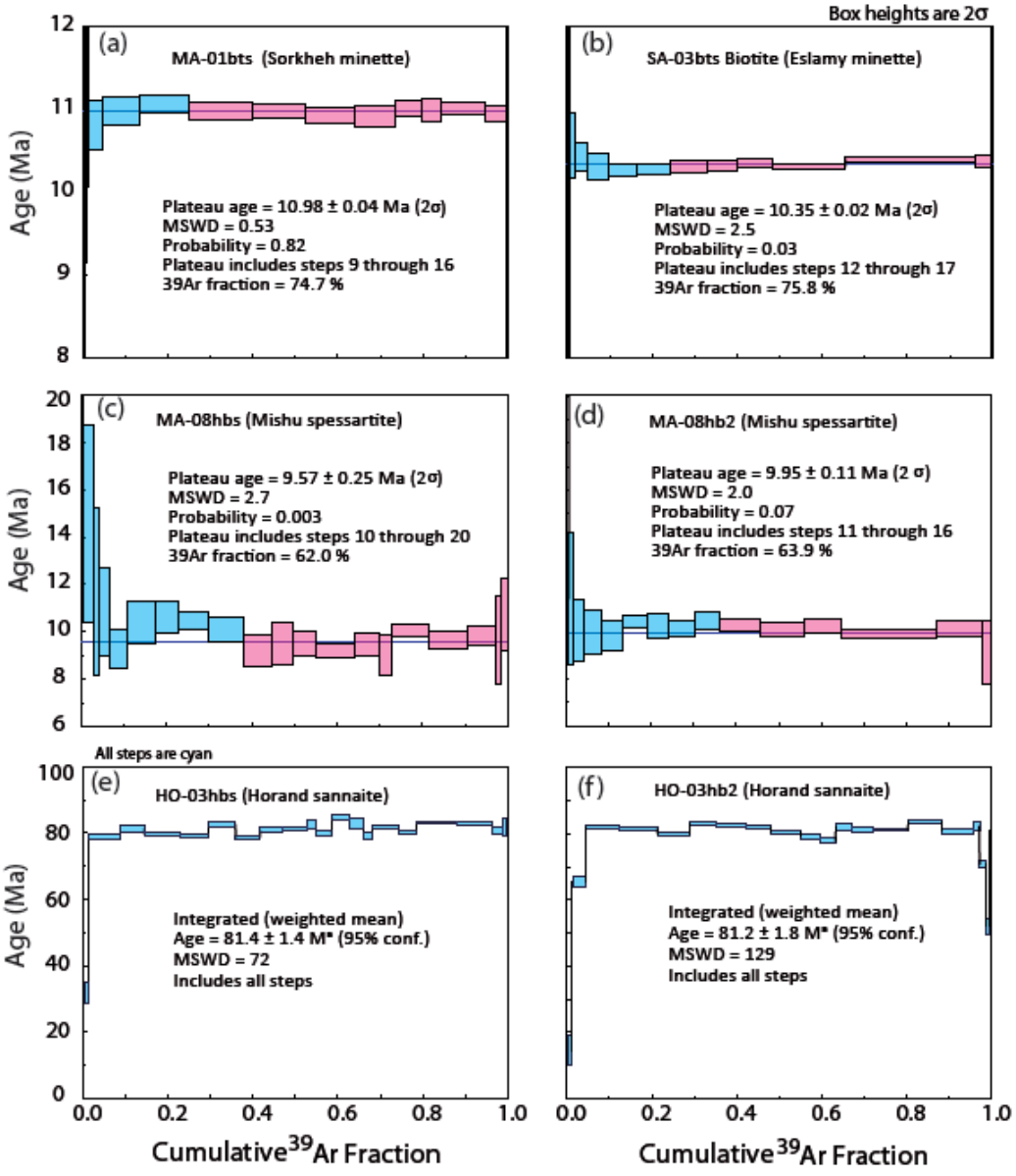

Figure 5

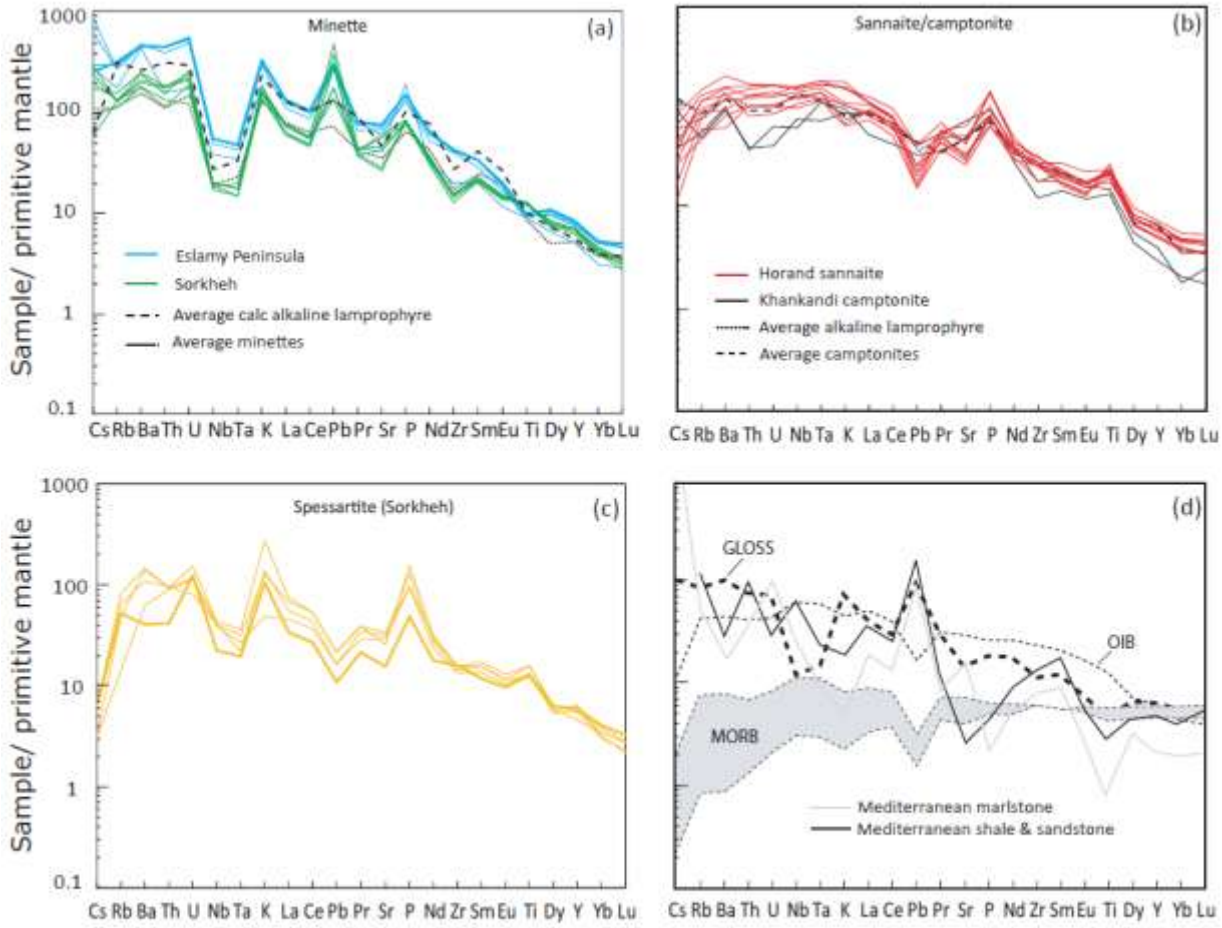

Figure 6

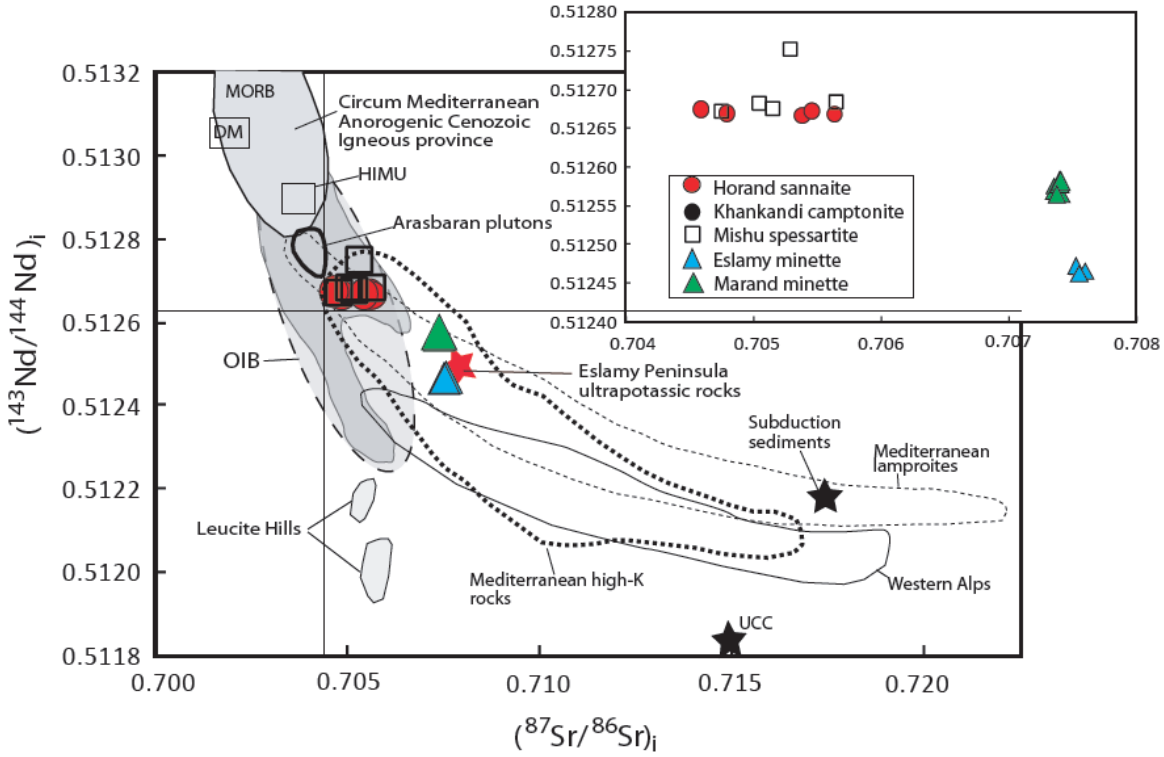

Figure 7

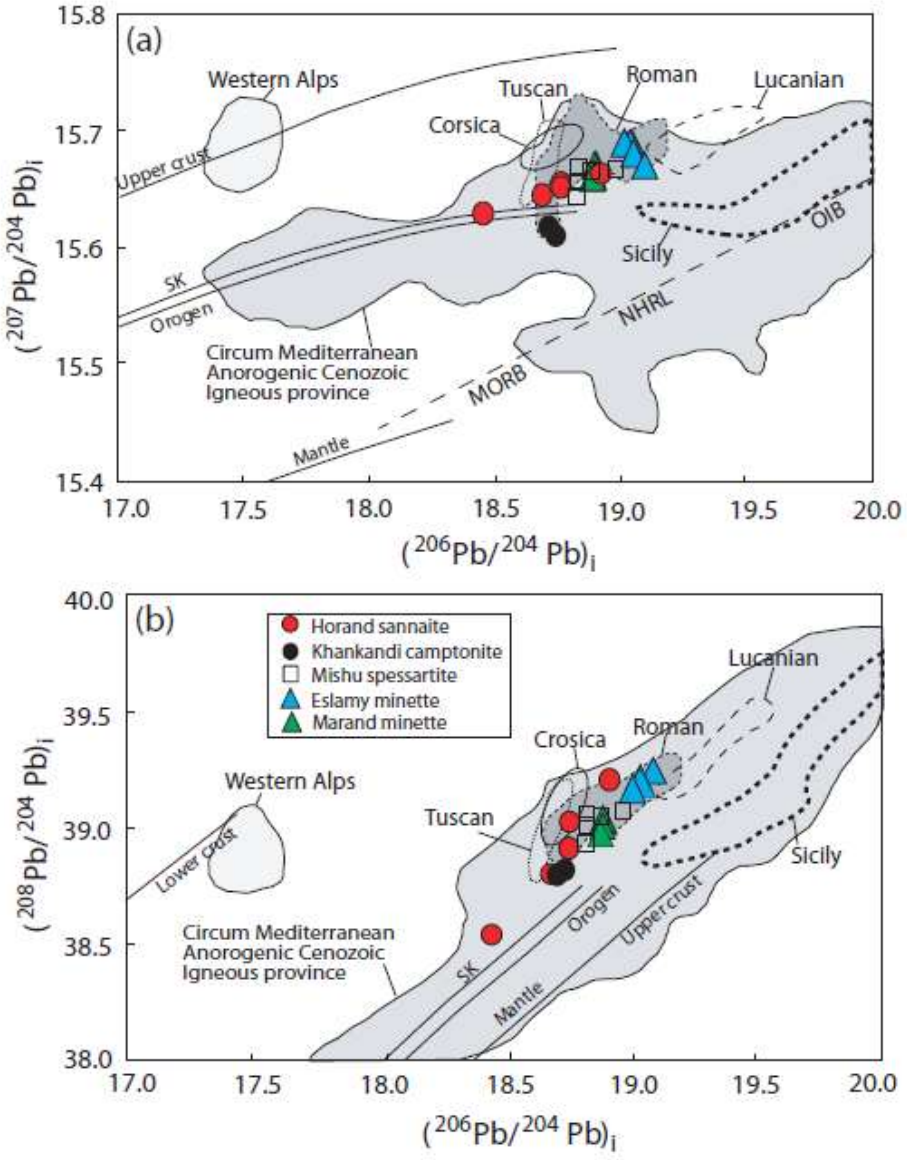

Figure 8

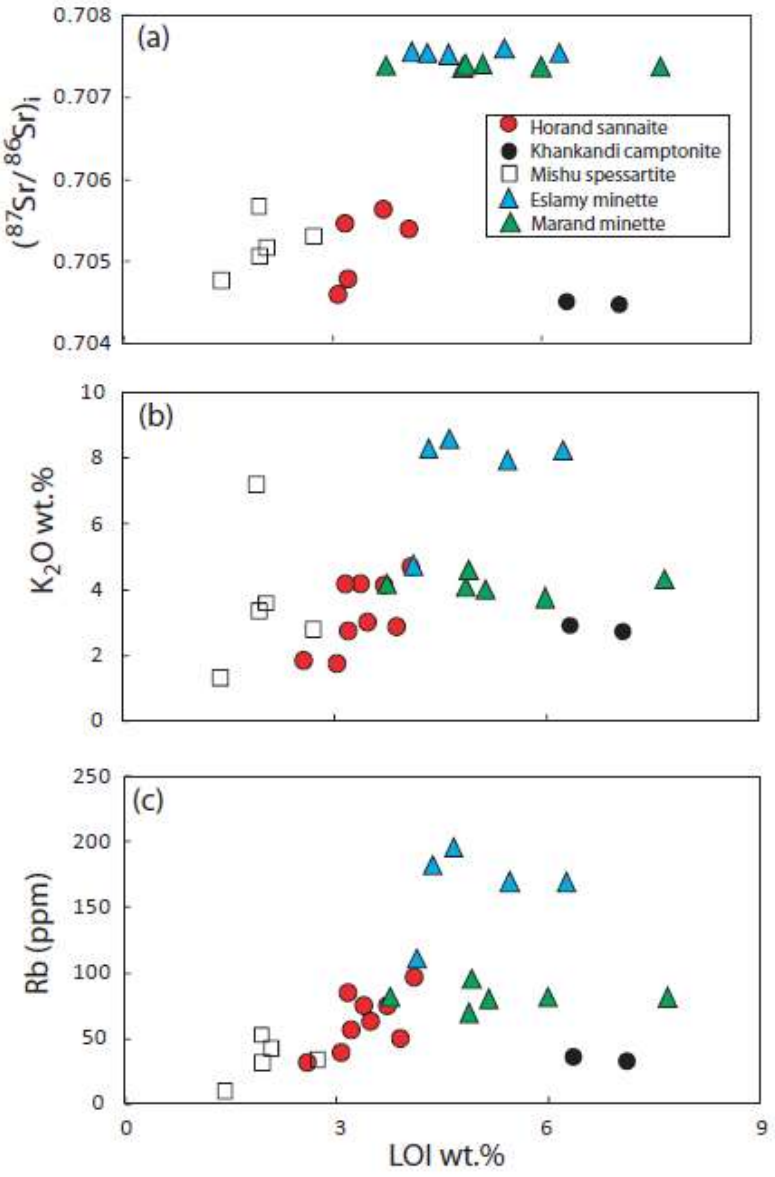

Figure 9

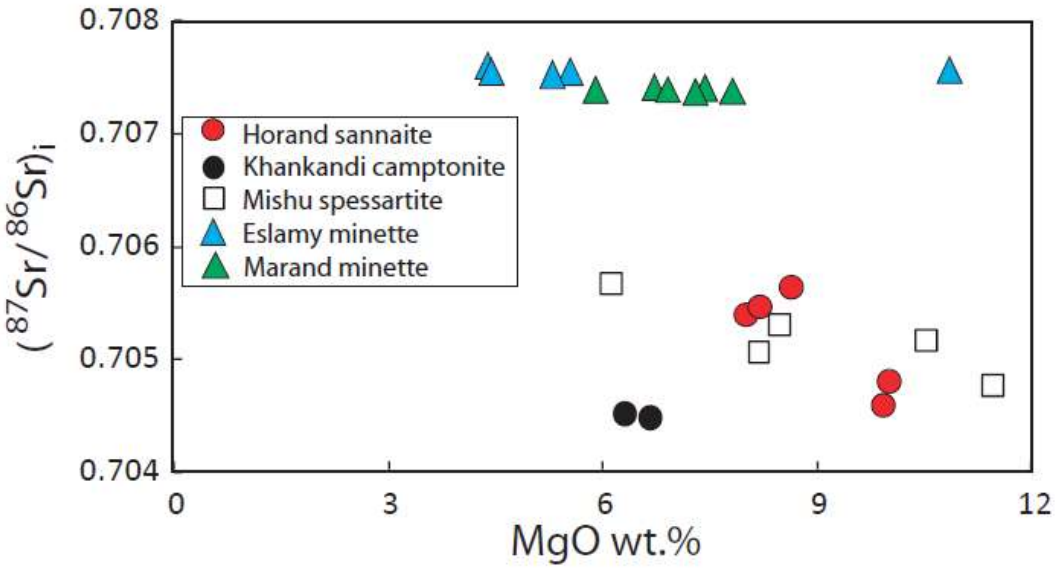

Figure 10

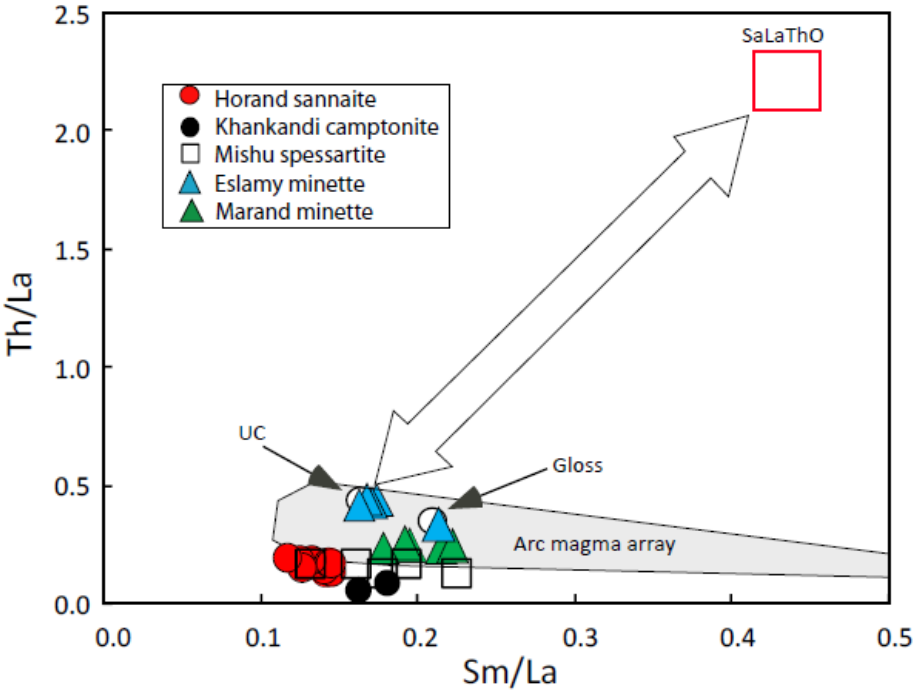

Figure 11

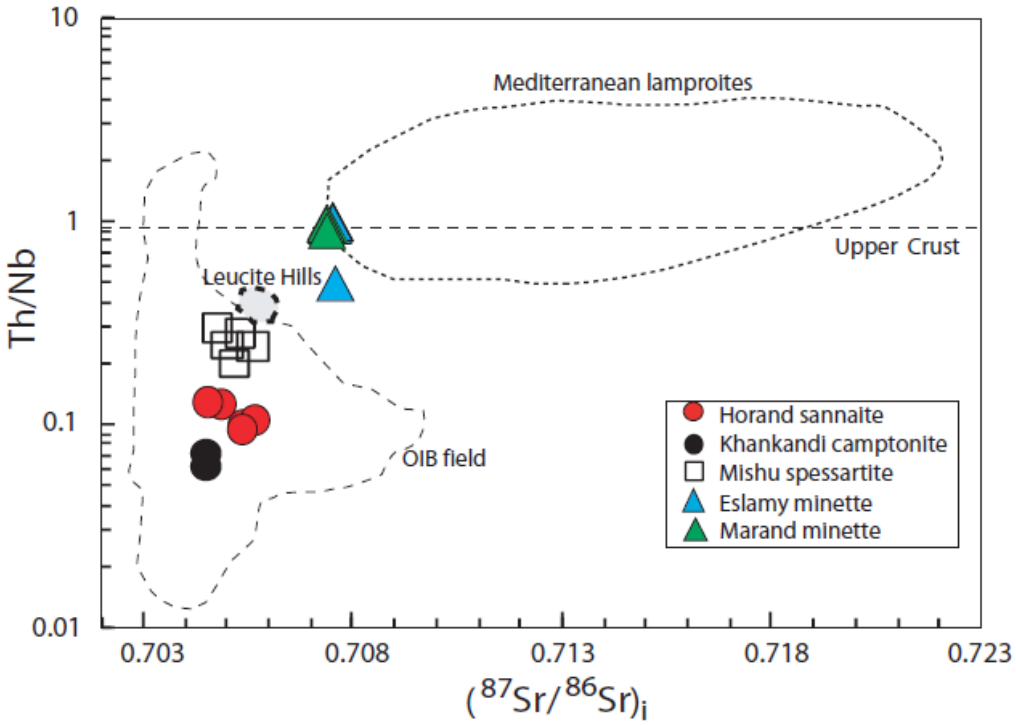

Figure 12

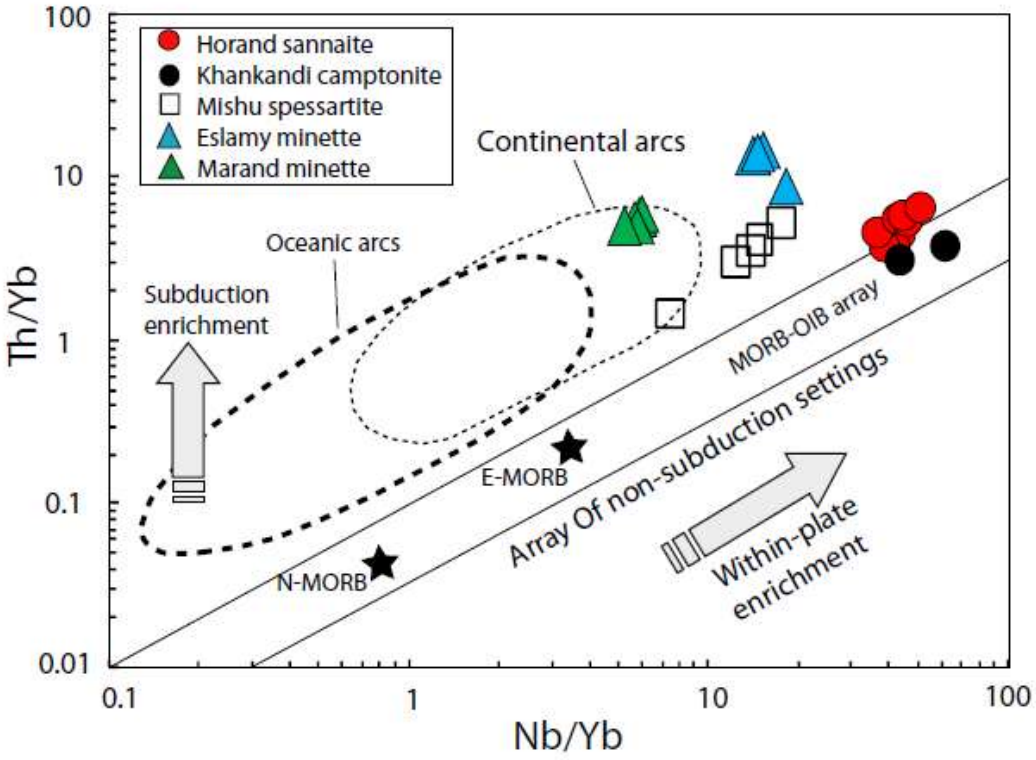

Figure 13

Table 1 - Selected microprobe analyses of mineral phases of studied Lamprophyres.

Mineral	Amphibole								Clinopyroxene												Mica							
	Sannaite					Camptonite			Sannaite		Camptonite		Spessartite			Minette					Minette							
Area	Horand					Khankandi			Horand		Khankandi		Sorkheh			Eslamy		Sorkheh			Eslamy				Sorkheh			
SiO2	38.6*	38.9	39.8	38.9*	39.2	38.9*	39.7*	SiO2	48.7*	47.3	47.8*	48.7*	51.6*	47.4	46.7	54.3*	50.0	50.9*	49.9*	45.6	SiO2	36.9*	37.4	36.7	39.1*	33.8	35.2*	34.3	34.3
TiO2	5.89	4.99	4.35	5.60	5.06	5.23	5.48	TiO2	1.94	1.52	2.00	1.50	0.70	1.63	1.64	0.20	1.07	0.56	0.73	1.71	TiO2	3.08	3.35	3.89	2.05	5.14	4.11	4.54	4.58
Al2O3	13.9	12.9	12.3	13.4	12.5	12.8	12.7	Al2O3	4.60	4.80	6.02	4.10	2.79	5.69	5.79	0.57	2.57	2.17	2.82	6.73	Al2O3	14.6	14.3	13.9	13.6	13.5	15.5	14.7	14.7
FeO	11.6	12.9	14.4	11.6	13.2	9.31	9.38	Fe_2O_3**	3.76	4.17	2.03	1.60	4.05	5.84	5.69	0.72	4.21	1.33	2.12	4.03	Fe_2O_3**	0.00	0.00	0.00	0.00	0.00	0.00	0.00	0.00
MnO	0.10	0.17	0.24	0.17	0.15	0.04	0.08	FeO**	3.61	8.34	5.20	4.62	1.58	2.20	2.69	1.62	2.50	4.61	4.57	3.84	FeO**	8.40	9.11	10.4	5.28	17.8	9.91	12.4	14.1
MgO	12.1	11.5	10.8	12.1	11.2	14.13	14.2	MnO	0.14	0.39	bdl	bdl	0.13	0.14	0.18	0.11	0.15	0.14	0.09	0.10	MnO	0.13	0.04	0.09	0.02	0.55	0.16	0.13	0.25
CaO	11.8	11.7	11.5	11.6	11.5	11.9	11.9	MgO	13.8	9.72	13.7	14.3	16.1	13.3	12.9	18.1	14.8	15.0	14.4	12.2	MgO	20.9	20.1	18.5	23.3	11.6	17.6	15.3	13.9
Na2O	2.45	2.61	2.64	2.31	2.52	2.40	2.31	CaO	23.0	22.6	22.9	23.0	23.5	23.1	23.1	23.8	23.3	22.5	22.4	22.3	CaO	0.00	0.02	0.02	0.00	0.02	0.06	0.01	0.00
K2O	1.33	1.24	1.33	1.31	1.31	1.17	1.17	Na2O	0.46	0.62	bdl	bdl	0.41	0.54	0.38	0.20	0.33	0.22	0.28	0.39	Na2O	0.41	0.42	0.46	0.22	0.45	0.75	0.74	0.74
								K2O	0.01	0.01	bdl	bdl	0.00	0.00	0.03	0.00	0.02	0.01	0.00	0.00	K2O	9.20	8.70	9.11	10.15	7.70	8.28	8.22	8.35
																					$H2O^{+***}$	4.06	4.06	3.99	4.12	3.74	3.94	3.83	3.82
sum	98.2	97.3	97.7	97.4	96.9	96.5	97.7	sum	100.02	99.48	99.64	97.82	100.81	99.83	99.10	99.90	99.00	97.44	97.31	96.89	Sum	97.67	97.54	97.07	97.80	94.30	95.51	94.14	94.75
Atomic proportions on the basis of 15 cations and Fe3+ from stoichiometry								*Atomic proportions on the basis of 4 cations and Fe3+ from stoichiometry*													*Cations on the basis of 24 (O, OH, F, Cl), and Fe3+ from stoichiometry*							
Si	5.797	5.926	6.079	5.883	6.005	5.861	5.918	Si	1.809	1.811	1.783	1.843	1.880	1.767	1.759	1.952	1.934	1.925	1.896	1.754	Si IV	5.456	5.530	5.513	5.693	5.419	5.351	5.366	5.381
Al^{IV}	2.203	2.074	1.921	2.117	1.995	2.139	2.082	Al	0.191	0.189	0.217	0.157	0.120	0.233	0.241	0.048	0.053	0.075	0.104	0.246	Al IV	2.543	2.470	2.461	2.307	2.551	2.649	2.634	2.619
Ti	0.000	0.000	0.000	0.000	0.000	0.000	0.000	Ti	0.000	0.000	0.000	0.000	0.000	0.000	0.000	0.000	0.011	0.000	0.000	0.000	Fe3+ IV	0.000	0.000	0.000	0.000	0.000	0.000	0.000	0.000
Fe3+	0.000	0.000	0.000	0.000	0.000	0.000	0.000	Fe3+	0.000	0.000	0.000	0.000	0.000	0.000	0.000	0.000	0.003	0.000	0.000	0.000	Ti IV	0.001	0.000	0.027	0.000	0.029	0.000	0.000	0.000
Al^{VI}	0.257	0.242	0.294	0.272	0.262	0.134	0.150	Al	0.011	0.028	0.048	0.026	0.000	0.017	0.016	0.004	0.000	0.022	0.022	0.059	Al VI	0.000	0.029	0.000	0.019	0.000	0.128	0.072	0.095
Ti	0.665	0.572	0.500	0.637	0.583	0.593	0.614	Ti	0.054	0.044	0.056	0.043	0.019	0.046	0.046	0.012	0.000	0.016	0.021	0.049	Ti VI	0.341	0.372	0.413	0.224	0.590	0.470	0.534	0.540
Mg	2.709	2.612	2.459	2.728	2.558	3.174	3.156	Fe3+	0.105	0.120	0.057	0.045	0.111	0.164	0.161	0.034	0.070	0.038	0.061	0.117	Fe3+	0.000	0.000	0.000	0.000	0.000	0.000	0.000	0.000
Fe2+	1.457	1.643	1.834	1.462	1.691	1.173	1.169	Mg	0.764	0.555	0.762	0.807	0.872	0.739	0.724	0.911	0.942	0.846	0.816	0.700	Fe2+	1.039	1.127	1.308	0.643	2.387	1.260	1.621	1.854
Mn	0.013	0.022	0.031	0.022	0.019	0.005	0.010	Fe2+	0.112	0.267	0.162	0.146	0.048	0.068	0.085	0.076	0.034	0.146	0.145	0.123	Mn	0.016	0.005	0.011	0.002	0.075	0.021	0.017	0.033
Ca	1.899	1.910	1.882	1.880	1.887	1.921	1.901	Mn	0.004	0.013	0.000	0.000	0.004	0.004	0.006	0.002	0.004	0.004	0.003	0.003	Mg	4.607	4.431	4.143	5.057	2.773	3.989	3.568	3.251
								Ca	0.916	0.927	0.915	0.933	0.917	0.923	0.932	0.947	0.935	0.912	0.912	0.919									
Na	0.713	0.771	0.782	0.677	0.748	0.701	0.668	Na	0.033	0.046	0.000	0.000	0.029	0.039	0.028	0.013	0.014	0.016	0.021	0.029	Ca	0.000	0.003	0.003	0.000	0.003	0.010	0.002	0.000
K	0.255	0.241	0.259	0.253	0.256	0.225	0.223	K	0.000	0.000	0.000	0.000	0.000	0.000	0.001	0.001	0.000	0.000	0.000	0.000	Na	0.118	0.120	0.134	0.062	0.140	0.221	0.224	0.225
																					K	1.735	1.641	1.746	1.885	1.575	1.606	1.640	1.671
								En	40.20	29.48	40.18	41.78	44.66	38.93	37.96	46.25	47.40	43.47	42.12	37.57								
								Fe	11.65	21.26	11.55	9.93	8.35	12.47	13.19	5.69	5.59	9.68	10.78	13.06	OH	4.000	4.000	4.000	4.000	4.000	4.000	4.000	4.000
								Wo	48.15	49.26	48.27	48.29	46.99	48.60	48.85	48.06	47.02	46.86	47.09	49.36								
Mg#	0.648	0.611	0.569	0.648	0.599	0.729	0.728	Mg#	0.775	0.581	0.777	0.808	0.842	0.757	0.742	0.890	0.895	0.818	0.796	0.742	Mg#	0.814	0.797	0.758	0.887	0.530	0.757	0.685	0.633

Legend: bdl = below detection limit; Mg# = $Mg/(Mg+Fe^{2+}+Fe^{3+})$; * =Points analyzed from core of minerals; **Fe2O3 and FeO are calculated on the basis of stoichiometry from Atomic proportins; *** = H2O+ is calculated on the basis of stoichiometry from Atomic proportions.

Table 2. Whole rock major- and trace-element analyses of studied lamprophyres.

Region	Arasbaran Region											Mishu Range					Mishu Range						Eslamy (Saray) Peninsula				
Locality	Horand									Khankandi		Sorkheh and Tasuj					Marand						Eslamy				
Rock type	Sannaite									Camptonite		Spessartite					Minette										
Sample	HO-01	HO-02	HO-03	HO-04	HO-05	HO-06	HO-07	HO-08	HO-09	Kh M6 13	Kh M4 98	MA-09	MA-08	MA-10	MA-11	MA-13	MA-01	MA-02	MA-03	MA-04	MA-05	MA-06	SA-01	SA-03	SA-05	SA-06	SA-07
SiO2 (wt.%)	47.7	45.6	44.4	44.2	41.1	44.3	43.2	42.9	41.8	40.1	42.1	46.2	47.6	47.6	45.2	44.4	43.2	44.4	42.2	45.5	44.2	44.9	47.8	46.8	43.9	44.8	45.2
TiO_2	2.45	3.05	3.16	3.04	3.68	3.22	2.93	3.36	2.68	2.07	1.85	1.72	1.66	1.57	2.05	2.07	1.58	1.59	1.63	1.57	1.67	1.56	1.15	1.27	1.20	1.19	1.25
Al_2O_3	16.4	15.8	15.1	14.1	12.0	15.2	14.1	12.5	13.0	12.3	13.1	12.2	14.4	14.5	14.2	12.5	13.2	13.5	12.4	13.5	13.1	12.9	9.32	13.3	13.1	13.4	13.1
$Fe_2O_{3\,TOT}$	9.86	10.9	11.2	13.3	15.8	10.9	13.1	14.6	12.4	8.24	8.84	10.3	10.0	9.55	10.2	10.9	11.2	11.7	11.5	11.3	12.0	11.2	8.73	10.3	9.75	9.80	10.1
FeO	nd	nd	nd	nd	nd	nd	nd	nd	nd	nd	nd	nd	nd	nd	nd	nd	nd	nd	nd	nd	nd	nd	nd	nd	nd	nd	nd
MnO	0.17	0.20	0.26	0.21	0.22	0.24	0.22	0.22	0.18	0.14	0.12	0.11	0.16	0.13	0.10	0.13	0.19	0.20	0.20	0.19	0.23	0.20	0.15	0.18	0.16	0.17	0.18
MgO	4.82	5.50	5.34	7.76	9.60	5.21	7.78	8.28	9.39	5.63	5.37	11.2	8.17	5.91	7.92	10.2	5.33	6.32	6.72	6.59	7.35	7.00	10.6	5.35	3.95	4.07	4.96
CaO	6.11	8.12	8.85	8.11	10.00	8.48	7.08	9.36	9.26	10.48	7.87	10.2	7.87	8.45	9.80	9.77	8.58	8.81	10.7	9.35	8.10	9.04	12.2	9.29	8.46	8.39	8.89
Na_2O	2.80	2.60	2.10	2.70	2.00	2.03	2.80	2.32	1.72	2.28	2.41	3.50	3.10	0.80	2.60	2.00	2.50	3.00	2.60	2.70	2.60	2.40	1.20	0.70	1.20	0.80	0.60
K_2O	4.51	4.05	3.95	2.67	1.67	3.95	2.83	1.75	2.68	2.28	2.44	1.24	2.65	6.92	3.20	3.48	3.89	3.77	3.43	3.98	3.85	4.35	4.60	8.01	7.15	7.55	8.06
P_2O_5	0.98	1.33	1.43	0.81	0.64	1.36	0.75	0.64	0.82	0.93	0.82	0.91	0.46	0.93	1.48	1.23	0.79	0.78	0.74	0.72	0.77	0.71	1.81	1.42	1.20	1.20	1.39
LOI	4.09	3.17	3.72	3.21	3.06	3.39	3.48	2.58	3.90	7.10	6.36	1.41	2.73	1.93	1.96	2.07	7.69	5.15	5.99	3.76	4.87	4.91	4.13	4.35	5.46	6.25	4.65
Sum	100.0	100.3	99.50	100.1	99.70	96.50	98.40	98.60	98.00	98.90	99.40	99.00	98.80	98.30	98.70	98.80	98.20	99.20	98.20	99.20	98.70	99.20	101.7	101.1	95.60	97.60	98.40
Mg#	52.6	53.4	52.0	57.0	58.0	52.0	57.5	56.4	63.3	60.8	58.0	71.2	65.0	58.4	63.8	68.0	51.9	55.1	57.0	57.0	58.2	58.6	73.4	54.1	47.9	48.5	52.7
ne	1.77	4.63	3.32	4.79	5.49	2.19	5.58	3.08	4.62	6.46	0.24	7.10	3.44	3.84	6.19	6.80	8.86	11.59	13.08	10.31	9.01	10.34	4.26	3.35	6.17	4.05	2.96
lc	0.00	0.00	0.00	0.00	0.00	0.00	0.00	0.00	0.00	0.00	0.00	0.00	0.00	2.08	0.00	0.00	0.00	0.00	0.00	0.00	0.00	0.00	3.72	18.72	13.93	13.77	21.83
V (ppm)	131	168	218	220	320	294	319	398	293	207	154	241	166	184	226	228	353	336	318	305	337	314	190	253	231	250	280
Cr	nd	nd	nd	nd	nd	30	150	180	300	250	188	212	209	189	79	61	45	50	100	60	75	76	nd	nd	nd	nd	nd
Co	21.1	25.1	29.0	37.2	51.9	30.2	44.3	52.0	51.2	39.6	34.1	48.0	40.0	34.0	35.0	37.0	40.0	39.0	43.0	40.0	44.0	42.0	37.6	31.0	27.2	30.3	31.2
Ni	10	21	41	67	106	31	98	119	230	142	91	131	112	100	57	68	34	36	54	39	47	46	86	32	21	26	33
Ga	20	19	22	20	22	23	22	21	17	20	30	17	19	18	20	18	17	20	18	19	20	21	14	20	19	20	20
Rb	96.9	84.9	74.8	57.0	39.6	74.8	62.7	31.1	49.7	32.8	36.3	9.0	33.0	53.0	31.0	42.0	81	80	82	82	69	96	111	183	169	169	196
Sr	1120	1400	950	720	580	933	664	743	632	1610	1066	621	331	723	544	663	1233	841	545	1169	585	934	880	1490	1380	1250	1540
Y	29.0	32.1	32.2	25.3	23.7	35.1	28.6	26.8	23.6	19.1	14.1	26.0	27.0	21.0	25.0	29.0	32.0	32.0	28.0	30.0	30.0	31.0	22.8	36.4	33.8	35.0	37.1
Zr	380	370	360	330	300	324	313	293	214	210	143	148	179	177	175	161	169	166	140	170	156	170	220	480	440	450	460
Nb	117	111	110	89.0	73.0	120	105	92.3	79.0	56.3	45.5	28	16	31	29	29	14	13	12	14	13	14	27	38	34	38	38
Cs	2.80	2.20	1.20	1.00	0.40	1.39	1.53	0.90	0.59	3.02	1.30	0.1	0.2	0.2	0.1	0.2	1.8	7.5	6.1	9.1	3.4	5.3	8.7	9.3	27	19	7.9
Ba	1460	1120	950	680	450	1110	852	596	1015	682	722	440	281	1024	1005	757	1639	1350	1191	1458	1230	1675	3020	3230	3270	3030	3110
La	77.8	79.2	77.0	64.4	53.7	88.9	75.5	65.5	57.9	62.9	37.0	31.6	23.5	52.4	47.1	38.9	51.7	51.7	40.1	48.1	42.4	50.9	40.6	84.9	75	86.9	89.8
Ce	141	147	147	118	96.2	175	141	125	111	128	78.9	66.3	48.2	95.2	94.2	77.8	96.2	101	81.6	94.8	85.2	98.2	80.6	172	150	175	179
Pr	15.7	16.4	16.8	13.0	11.0	19.8	15.6	14.2	12.6	15.7	10.5	8.01	5.93	10.7	11.1	9.50	11.3	12.1	10.1	11.4	10.6	11.9	10.2	20.6	17.9	21.2	21.9
Nd	55.0	61.7	62.5	47.9	41.9	70.9	53.0	49.7	45.0	58.2	39.9	32.1	24.1	40.4	42.5	36.9	44.7	50.0	40.5	45.7	43.3	47.0	42.0	80.4	69.0	80.7	83.8
Sm	9.20	10.5	11.0	8.10	7.80	12.9	9.59	9.15	8.21	10.2	6.65	6.1	5.3	6.9	7.6	6.9	9.2	10.1	8.9	9.4	9.1	9.8	8.7	14.8	12.6	14.8	14.6
Eu	2.80	3.05	3.06	2.42	2.29	3.90	3.01	2.82	2.48	2.79	2.11	1.75	1.64	1.94	2.20	1.92	2.32	2.53	2.23	2.33	2.30	2.44	1.94	3.16	2.73	3.05	3.26
Gd	7.07	8.17	8.47	6.11	6.18	12.50	9.53	9.03	8.17	7.97	5.15	4.95	4.72	5.54	6.29	5.24	7.42	8.44	7.48	7.66	7.55	7.75	6.90	10.60	9.48	10.40	10.90
Tb	1.03	1.19	1.21	0.94	0.91	1.60	1.26	1.24	1.11	0.92	0.69	0.68	0.77	0.74	0.85	0.74	1.07	1.10	1.01	1.05	1.02	1.08	0.94	1.44	1.28	1.42	1.49
Dy	5.91	6.51	6.49	5.29	4.98	7.66	6.13	6.01	5.19	4.28	3.39	3.97	4.58	4.30	4.79	4.25	5.36	6.16	5.37	5.74	5.55	5.92	4.72	7.51	6.87	7.24	7.83
Ho	1.13	1.19	1.25	0.97	0.96	1.41	1.16	1.11	0.98	0.75	0.58	0.76	0.92	0.82	0.88	0.77	0.98	1.14	0.99	0.96	0.97	1.02	0.81	1.32	1.22	1.29	1.36
Er	2.76	3.04	3.08	2.50	2.41	3.53	2.82	2.85	2.44	1.88	1.35	1.92	2.47	2.21	2.27	2.14	2.51	2.81	2.45	2.63	2.42	2.81	2.05	3.22	3.11	3.17	3.20
Tm	0.40	0.41	0.41	0.34	0.33	0.44	0.37	0.37	0.28	0.22	0.17	0.25	0.34	0.29	0.31	0.28	0.33	0.36	0.33	0.32	0.32	0.37	0.23	0.43	0.38	0.41	0.41
Yb	2.30	2.50	2.40	2.10	2.00	2.88	2.43	2.39	1.90	0.92	1.06	1.5	2.0	1.7	1.9	1.6	2.0	2.2	1.9	2.1	1.9	2.2	1.5	2.5	2.4	2.6	2.5
Lu	0.34	0.36	0.35	0.27	0.26	0.41	0.36	0.32	0.28	0.19	0.13	0.17	0.24	0.20	0.21	0.16	0.25	0.26	0.23	0.22	0.20	0.24	0.21	0.34	0.33	0.34	0.36
Hf	8.0	7.0	7.0	7.0	7.0	7.1	7.1	7.1	5.2	4.7	4.2	4	4	4	4	4	4	4	4	4	4	4	6	10	9	11	7
Ta	7.6	7.1	7.0	5.9	4.9	7.7	6.6	6.0	5.2	3.1	4.7	1.1	0.8	1.5	1.3	0.9	0.7	0.8	0.6	0.7	0.6	0.7	1.4	1.9	1.7	1.9	1.9
Pb	4.0	3.4	4.0	4.5	3.0	8.0	8.0	3.0	5.0	8.2	6.4	3	2	4	4	3	24	69	51	32	53	86	32	25	49	49	54
Th	14.9	14.1	13.2	11.7	9.10	11.5	10.9	9.10	7.22	3.49	3.29	7.7	3.5	8.1	7.9	8.3	12.8	14.6	9.5	14.9	11.3	15.2	13.3	37.0	32.2	36.7	37.0
U	3.58	3.57	3.50	3.07	2.17	2.86	2.77	2.30	1.86	0.90	1.36	2.4	2.6	3.2	2.5	1.7	5.3	4.3	3.8	5.0	2.5	4.5	3.5	10.8	10.1	11.0	11.2
Th/Nb	0.13	0.13	0.12	0.13	0.12	0.10	0.10	0.10	0.09	0.06	0.07	0.28	0.22	0.26	0.27	0.29	0.91	1.12	0.79	1.06	0.87	1.09	0.49	0.97	0.95	0.97	0.97
K2O/Na2O	1.61	1.56	1.88	0.99	0.84	1.95	1.01	0.75	1.56	1.00	1.01	0.35	0.85	8.65	1.23	1.74	1.56	1.26	1.32	1.47	1.48	1.81	3.83	11.44	5.96	9.44	13.43
Sum REE	322.44	341.22	341.02	272.34	230.92	401.28	321.71	289.64	257.49	294.92	187.55	160.06	124.71	223.34	222.20	187.10	235.34	249.90	203.19	232.41	212.83	241.63	201.40	403.22	352.30	408.52	420.41

Legend: nd = not determined; Mg# = [MgO]/([MgO]+0.85*[FeO_{TOT}]); *ne* = normative nepheline; *lc* = normative leucite.

Table 3: Whole-rock Rb, Sr, Nd, Sm, Pb, U and Th content (ppm) and Sr, Nd and Pb isotope data for selected samples

District	Arasbaran				Mishu					Eslamy (Saray)					Mishu					
Locality	Khankandi				Horand					Sorkhab					Eslamy peninsula					Marand					
Unit	Comptonite				Sannaite					Spessartite					Minette					Minette					
Age (Ma)	23	11	23	11	81.4 ± 1.4					9.95 ± 0.11					10.35 ± 0.02					10.98 ± 0.04					
Sample	Kh-M4-98		Kh-M6-13		HO-01	HO-02	HO-03	HO-04	HO-05	MA-08	MA-09	MA-10	MA-11	MA-13	SA-01	SA-03	SA-05	SA-06	SA-07	MA-01	MA-02	MA-03	MA-04	MA-05	MA-06
Rb	36.3		32.8		96.9	84.9	74.8	57	39.6	33	9	53	31	42	111	183	169	169	196	81	80	82	82	69	96
Sr	1066		1610		1120	1400	950	720	580	331	621	723	544	663	880	1490	1380	1250	1540	1233	841	545	1169	585	934
Sm	6.7		10.2		9.2	10.5	11	8.1	7.8	5.3	6.1	6.9	7.6	6.9	8.7	14.8	12.6	14.8	14.6	9.2	10.1	8.9	9.4	9.1	9.8
Nd	39.9		58.2		55	61.7	62.5	47.9	41.9	24.1	32.1	40.4	42.5	36.9	42	80.4	69	80.7	83.8	44.7	50	40.5	45.7	43.3	47
Pb	6.39		8.2		4	3.4	4	4.5	3	2	3	4	4	3	32	25	49	49	54	24	69	51	32	53	86
Th	3.3		3.5		14.9	14.1	13.2	11.7	9.1	3.5	7.7	8.1	7.9	8.3	13.3	37	32.2	36.7	37	12.8	14.6	9.5	14.9	11.3	15.2
U	1.4		0.9		3.6	3.6	3.5	3.1	2.2	2.6	2.4	3.2	2.5	1.7	3.5	10.8	10.1	11	11.2	5.3	4.3	3.8	5	2.5	4.5
$(^{87}Sr/^{86}Sr)_i$	0.704507	0.704524	0.704477	0.704487	0.705398	0.705455	0.705634	0.704790	0.704590	0.705290	0.704758	0.705653	0.705049	0.705151	0.707559	0.707540	0.707603	0.707545	0.707522	0.707380	0.707408	0.707367	0.707393	0.707370	0.707402
2s.e.	0.000007	0.000006	0.000006	0.000006	0.000042	0.000030	0.000036	0.000039	0.000034	0.000008	0.000006	0.000007	0.000007	0.000007	0.000011	0.000010	0.000010	0.000010	0.000010	0.000007	0.000008	0.000011	0.000008	0.000010	0.000009
$(^{143}Nd/^{144}Nd)_i$	nc		nc		0.512667	0.512672	0.512669	0.512668	0.512674	0.512752	0.512672	0.512683	0.512682	0.512676	0.512463	0.512470	0.512466	0.512463	0.512472	0.512564	0.512582	0.512573	0.512580	0.512570	0.512567
2s.e.	nc		nc		0.000009	0.000009	0.000010	0.000009	0.000009	0.000005	0.000006	0.000005	0.000006	0.000009	0.000004	0.000004	0.000004	0.000004	0.000004	0.000005	0.000004	0.000005	0.000005	0.000005	0.000005
μ	14.0		7.0		59.1	69.5	57.8	45.6	48.3	81.4	51.8	51.8	40.3	36.7	7.1	28.0	13.4	14.6	13.4	14.3	4.0	4.8	nc	3.1	3.4
$(^{206}Pb/^{204}Pb)_i$	18.701	18.727	18.735	18.748	18.678	18.442	18.753	18.917	18.750	18.822	18.875	18.826	18.832	18.970	19.102	19.016	19.049	19.049	19.041	18.883	18.893	18.902	nc	18.899	18.881
2.se.	0.013	0.011	0.011	0.011	0.107	0.130	0.106	0.086	0.091	0.021	0.016	0.016	0.014	0.013	0.011	0.012	0.012	0.011	0.011	0.011	0.011	0.011	nc	0.011	0.011
$(^{207}Pb/^{204}Pb)_i$	15.614	15.616	15.613	15.613	15.645	15.629	15.654	15.660	15.651	15.643	15.664	15.660	15.664	15.665	15.672	15.683	15.681	15.688	15.684	15.657	15.663	15.670	nc	15.673	15.657
2.se.	0.014	0.014	0.014	0.013	0.014	0.015	0.014	0.014	0.015	0.014	0.013	0.014	0.014	0.015	0.014	0.014	0.014	0.014	0.014	0.014	0.014	0.014	nc	0.015	0.014
$(^{208}Pb/^{204}Pb)_i$	38.786	38.806	38.818	38.834	38.798	38.542	39.026	39.209	38.916	38.921	39.047	39.012	39.051	39.070	39.246	39.163	39.188	39.206	39.187	38.976	38.998	39.023	nc	39.035	38.976
2.se.	0.028	0.027	0.027	0.028	0.155	0.169	0.136	0.111	0.126	0.028	0.030	0.029	0.029	0.031	0.028	0.028	0.030	0.028	0.028	0.028	0.027	0.027	nc	0.029	0.028

Footnote: Ma: million year. Standard errors (2 s.e.) on initial isotope ratios are propagated through a Monte-Carlo simulation assuming 5 % error on Rb, Sr, Sm, Nd, Pb, Th and U concentrations. nc: not calculated.

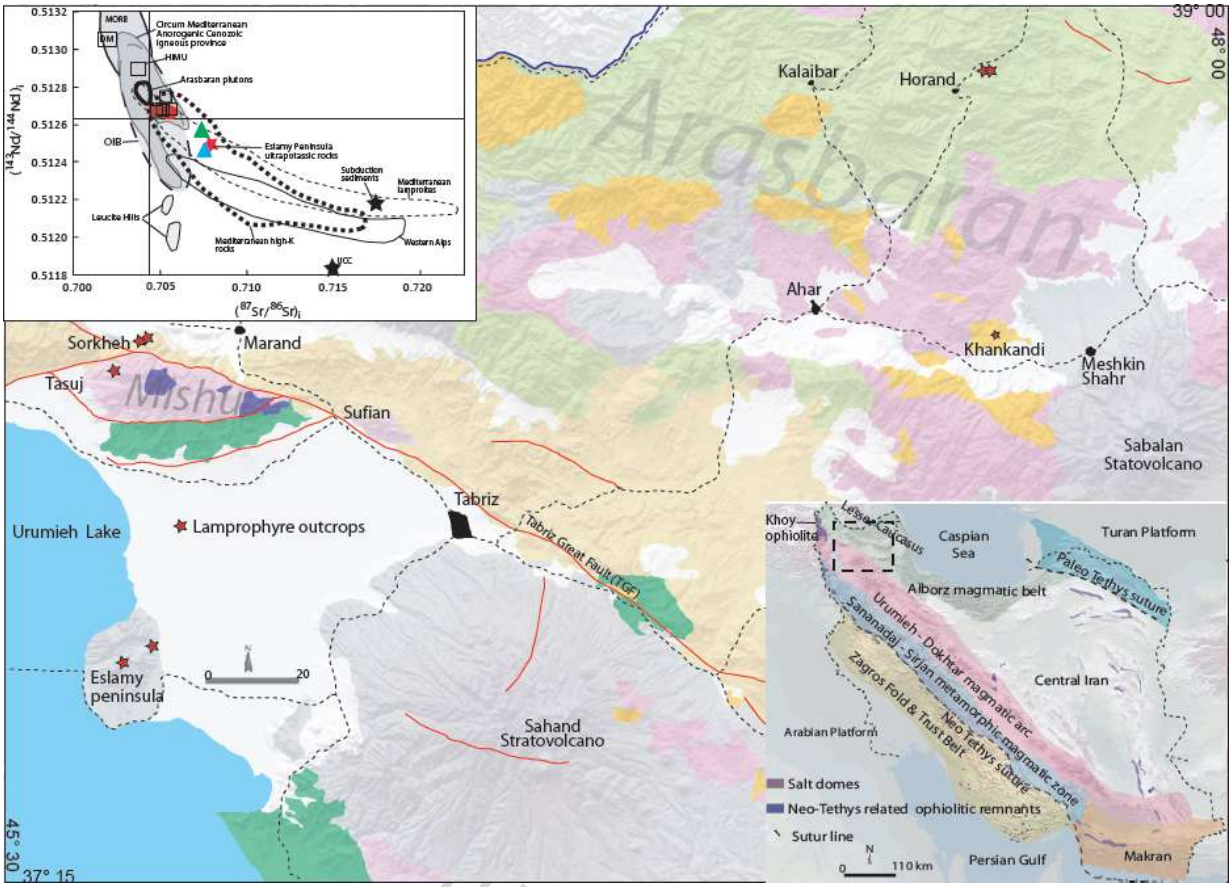

Graphical abstract

Highlights

-Northwestern Iranian lamprophyres have alkaline and calc-alkaline nature.

-Studied lamprophyres are emplaced during Late Cretaceous to Late Miocene time.

-Lamprophyres originated from different metasomatised lithospheric mantle.